nature communications

Article

https://doi.org/10.1038/s41467-026-73266-y

Cholecystokinin input from the anterior cingulate cortex to the lateral periaqueductal gray mediates nocebo pain behavior in mice

Received: 21 April 2025

Accepted: 7 May 2026

Published online: 20 May 2026

Check for updates

Sandra J. Poulson[1], Aleksandrina Skvortsova[2,3], Fatama Tuz Zahra[4], Damien C. Boorman[1], Seyed Asaad Karimi[1], Lisiê V. Paz[1], Wanning Cui[1], Antonietta Mandatori[1], Jacob Burek[1], Zahra Siddiqi[1], Maryam I. Fazili[4], Shivani R. Gami[1], Oakley B. Morgan[2,3], Mélanie Di Maria[2,3], Anton Dinh[1], Lianfang Liang[2], Robert Contofalsky[2], Jeffrey S. Mogil[2,3] ✉ & Loren J. Martin[1,4] ✉

The nocebo effect, opposite of the better-known placebo effect, in which anticipation of harm worsens pain and other symptoms, is increasingly thought to be responsible for poor clinical outcomes. In humans, nocebo hyperalgesia (i.e., increased pain sensitivity) is blocked by proglumide, a cholecystokinin (CCK) receptor antagonist. Yet, the neural circuitry underlying nocebo hyperalgesia remains unidentified, largely due to a lack of appropriate animal models. Here, we developed distinct mouse models of CCK-dependent nocebo hyperalgesia in which the expectation of pain was elicited by contextual or social cues. We find that these nocebo paradigms share a neural circuit involving CCK release from neurons projecting from the anterior cingulate cortex to the lateral periaqueductal gray. This pathway could represent a promising target for therapeutic interventions in pain-related disorders.

Environmental and social cues are pivotal in shaping our perceptions of pain, influencing both placebo and nocebo effects[1–3]. Placebo analgesia arises when the positive expectation of pain relief triggers authentic analgesic outcomes, even without active painkillers—a concept widely explored in human studies[4–6] and recently in animals[7,8]. In the nocebo effect as it relates to pain, negative expectancies—created either by verbal suggestion, prior experience, or other contextual factors—lead to pain hypersensitivity or hyperalgesia[9]. Seminal work on nocebo hyperalgesia in humans by Benedetti and colleagues suggested that it was mediated by the peptide neurotransmitter cholecystokinin (CCK), as the CCK antagonist proglumide was able to abolish the nocebo effect (and potentiate placebo analgesia) in hidden injection experiments[10,11]. Very little is known about the biology of the nocebo effect beyond this due to the lack of appropriate animal models.

Rodents are capable of acquiring negative pain expectations both through direct associative learning[12,13] and through social observation[14,15], and both forms of learning can produce nocebo hyperalgesia in humans[2,16]. The anterior cingulate cortex (ACC), implicated in the aversive dimension of pain[17,18], is recruited during threat anticipation and defensive responding[19–22], positioning it as a key site for learned negative pain expectations. Expectation-dependent changes in pain engage descending modulatory circuits, suggesting that cortical regions encoding threat predictions may influence nociceptive processing via midbrain and brain stem pathways[23]. Consistent with this, the ACC contributes to descending

[1]Department of Psychological and Brain Sciences, University of Toronto Mississauga, Mississauga, ON, Canada. [2]Department of Psychology, McGill University, Montreal, QC, Canada. [3]Alan Edwards Centre for Research on Pain, McGill University, Montreal, QC, Canada. [4]Department of Cell and Systems Biology, University of Toronto, Toronto, ON, Canada. ✉e-mail: jeffrey.mogil@mcgill.ca; lj.martin@utoronto.ca

facilitation that biases brainstem and spinal circuits toward heightened sensitivity and pain-related action[24,25]. The ACC projects to the periaqueductal gray (PAG), a key hub for descending pain control, and human imaging studies suggest that nocebo responses engage rostral PAG regions distinct from those involved in placebo analgesia[26]. These findings implicate ACC–PAG circuitry in expectancy-driven pain hypersensitivity, but the cellular and neurochemical composition of this circuit remain unknown, and whether CCK signaling within this circuit contributes to nocebo hyperalgesia has not been tested.

Here, we describe experiments undertaken independently by two laboratories, investigating the neurochemistry underlying nocebo hyperalgesia produced either by conditioning mice to a context previously associated with tonic pain[12,27] or by social exposure to conspecifics in pain[15]. We hypothesized that environmentally conditioned and socially enhanced pain expectations rely on shared mechanisms that use CCK as a neurotransmitter. Using a combination of pharmacological, anatomical, and viral circuit-based approaches, we show that both phenomena depend on CCK receptor activation and identify a circuit involving CCKergic neurons projecting from the ACC to the lateral PAG that is required for nocebo hyperalgesia across paradigms.

Results

Inhibition of CCK receptors blocks nocebo pain hypersensitivity in mice

In humans, conditioning-based negative expectations have been shown to induce nocebo hyperalgesia[16,28]. Thus, we posited that prior exposure to pain coupled with subsequent presentation of cues associated with that pain would generate a negative expectation, leading to heightened pain sensitivity in mice, a phenomenon dependent on the CCK system. To test this, we used a conditioned pain hypersensitivity protocol that involved a single pairing of an unconditioned stimulus (UCS; hind paw incision, Fig. 1a) with a conditioned stimulus (CS; environmental context). In our protocol, mice were then returned to the same context 6 days later, after surgical incision sensitivity had resolved (Supplementary Fig. 1), to assess whether re-exposure to the pain-paired context was sufficient to elicit conditioned pain hypersensitivity. When unilateral hind paw incision pain was used as the UCS, robust mechanical hypersensitivity was observed after mice were returned to the same context (Fig. 1b), but not different context (Fig. 1c), an effect that was also observed for thermal hypersensitivity (Supplementary Fig. 2). Context-dependent hypersensitivity was blocked by systemic administration of proglumide, a nonspecific CCK receptor antagonist (Fig. 1d), and by the CCK-2-selective antagonist LY 225910 (Fig. 1e), consistent with a CCK-dependent contextual nocebo-like effect. Conditioned hypersensitivity was also present in the contralateral hind paw and was abolished by both antagonists (Supplementary Fig. 3), with the effect of LY 225910 replicated in CD-1 mice in an independent experiment (Supplementary Fig. 4).

Context-dependent hypersensitivity extinguished with repeated testing by day 9, whereas delaying context retrieval to day 9 still revealed the effect, which likewise extinguished with repeated testing sessions (Supplementary Fig. 5). To determine whether extinction could be induced by context re-exposure alone, separate cohorts were returned to the pain-paired context without test stimulus application

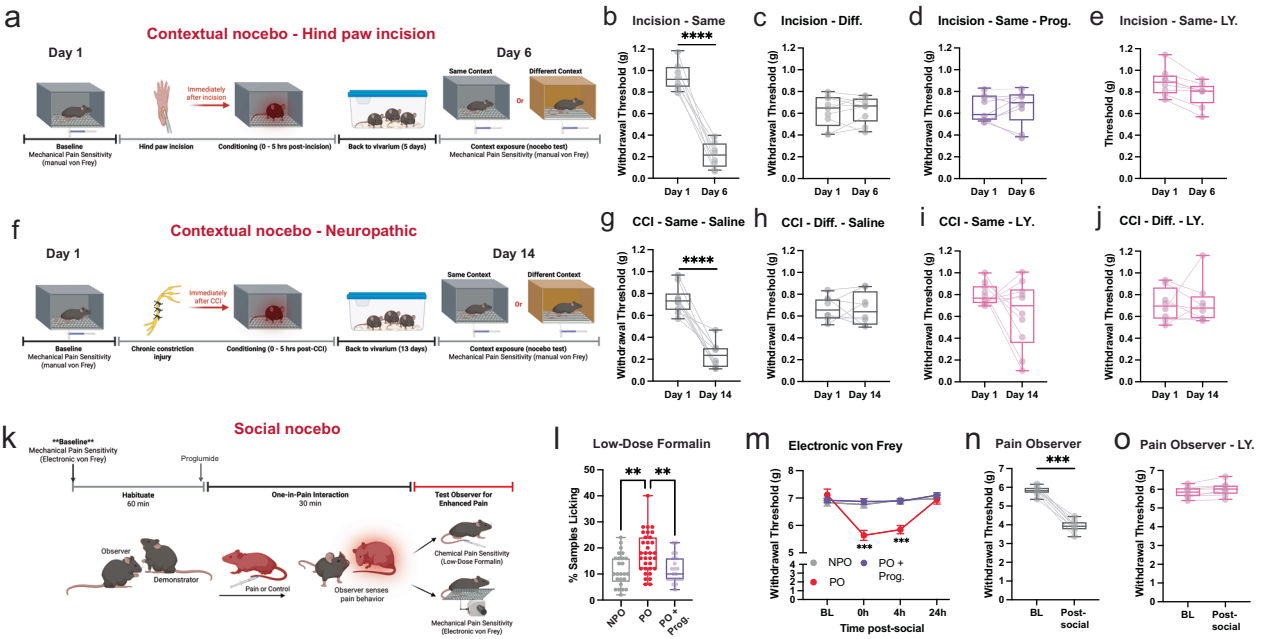

Fig. 1 | Contextual and social nocebo pain behavior in mice depends on cholecystokinin receptors. a Timeline of contextual nocebo conditioning using hind paw incision. Created in BioRender. Martin, L. (2026) https://BioRender.com/fpd01h4. Manual von Frey thresholds for C57BL/6 mice tested in the same context (**b** $n = 8$ mice, 4 M, 4 F), a different context (**c** $n = 9$ mice, 5 M, 4 F), the same context following proglumide (Prog.; **d** $n = 9$ mice, 5 M, 4 F), or LY 225910 (**e** $n = 8$ mice, 4 M, 4 F). **f** Timeline of contextual nocebo conditioning using chronic constriction injury (CCI). Created in BioRender. Martin, L. (2026) https://BioRender.com/ah2goxr. Manual von Frey thresholds in male CD-1 mice tested in the same context (**g** $n = 10$ mice), a different context (**h** $n = 8$ mice), the same context following LY 225910 (**i** $n = 10$ mice), or a different context following LY 225910 (**j** $n = 8$ mice). **k** Timeline of the social nocebo procedure. Created in BioRender. Martin, L. (2026) https://BioRender.com/o69o523. **l** Chemical sensitivity using a low-dose formalin assay in no pain observers (NPO, $n = 25$ mice, 15 M, 10 F), pain observers (PO, $n = 33$ mice, 23 M, 10 F), and PO + Prog. ($n = 21$ mice, 12 M, 9 F). **m** Electronic von Frey thresholds in male C57BL/6 mice at baseline (BL), 0, 4, and 24 h following social interaction; NPO ($n = 11$ mice), PO ($n = 12$ mice), and PO + Prog. ($n = 11$ mice). **n**, **o** Electronic von Frey thresholds in male C57BL/6 mice at baseline and post-social interaction in vehicle-treated ($n = 8$ mice) and LY 225910-treated mice ($n = 8$ mice). Box plots (**b**–**e**, **g**–**j**) show the median and interquartile range with paired measurements from individual mice. Symbols in (**l**, **m**) show mean ± SEM. Statistical analysis used two-way ANOVA (**b**–**e**, **l**–**o**); three-way ANOVA (**g**–**j**). $^{**}p < 0.01$, $^{***}p < 0.001$ from Šidák-corrected post hoc comparisons or paired two-sided t-tests with Bonferroni correction. Exact p values: **b** 8.1×10^{-14}; **g** 1.6×10^{-5}; **l** 0.0016 (NPO vs. PO) and 0.002 (PO vs. PO + Prog.); **m** 0 h: 2.54×10^{-7} (NPO vs. PO) and 8.0×10^{-9} (PO vs. PO + Prog.). 4 h: 6.7×10^{-7} (NPO vs. PO) and 1.12×10^{-6} (PO vs. PO + Prog.). **n** 4.68×10^{-12}. Full statistical reporting is provided in Supplementary Data 1. Source data are provided as a Source data file.

prior to assessment on day 6 (Supplementary Fig. 6a). Prolonged re-exposure (5 h per day) abolished context-dependent hypersensitivity, whereas shorter re-exposure (3 h per day) produced only a partial attenuation of the response (Supplementary Fig. 6b, c).

We next asked whether chronic constriction injury (CCI) of the sciatic nerve, a unilateral peripheral nerve injury producing neuropathic pain, could similarly produce conditioned pain hypersensitivity when mice were returned to the same context 14 days after injury (Fig. 1f). As with hind paw incision, mice tested in the CCI-paired context showed a significant reduction in mechanical withdrawal thresholds at day 14 (Fig. 1g), whereas no effect was observed in mice placed in a different context (Fig. 1h). Context-dependent hypersensitivity following CCI conditioning was likewise prevented by administration of the CCK-2-selective antagonist LY 225910 (Fig. 1i, j), and, as in the incision model, extended to the contralateral paw (Supplementary Fig. 7). Finally, independent cohorts showed no sex differences after either hind paw incision (Supplementary Fig. 8a–c) or CCI (Supplementary Fig. 8d–f) conditioning.

Since social cues, such as witnessing others in pain, also trigger nocebo hyperalgesia in humans[2,29] and facilitate pain in animals[14,15,30–33], we next sought to determine whether the CCK system also mediates the social enhancement of pain in mice. To address this, we adapted a one-in-pain social interaction assay in which a naïve mouse (i.e., pain observer, PO) interacted with a cagemate displaying signs of visible pain following an intraplantar injection of formalin (i.e., pain demonstrator, PD). PO mice were then subsequently tested for pain responses (either low-dose formalin or mechanical sensitivity) in the absence of PD mice (Fig. 1k). After social interaction, PO mice exhibited increased hind paw licking in response to a low-dose formalin injection compared to no pain observer (NPO) mice that interacted with a cagemate injected with saline (i.e., no pain demonstrator, NPD). Increased sensitivity in PO mice was blocked by systemic proglumide administration (Fig. 1l). PO mice showed increased mechanical sensitivity, measured using the electronic von Frey test, immediately and 4 h after social interaction, but not at 24 h. This effect was blocked by systemic proglumide (Fig. 1m) or LY 225910 (Fig. 1n, o) administered prior to social interaction. Proglumide administered after the social interaction similarly prevented the increase in pain sensitivity (Supplementary Fig. 9). During the 30-min social interaction, PD mice displayed overt hind paw licking, while NPD mice displayed little to no hind paw licking (Supplementary Fig. 10a). During social interaction, active attending behavior was increased in PO mice, which was not affected by proglumide (Supplementary Fig. 10b). However, PO mice showed increased propinquity (i.e., physical proximity) toward their social partner, which was blocked by proglumide (Supplementary Fig. 10c).

In addition to pain, nocebo is typically accompanied by anxiety, anticipatory fear, and stress[34], raising the possibility that CCK antagonism could reduce hypersensitivity by attenuating a generalized stress-related state. To determine whether CCK signaling contributes more broadly to stress- or fear-related pain modulation, we examined the effects of CCK antagonism in a predator-threat paradigm (Supplementary Fig. 11a) that elicits robust anxiety-like behavior and stress-evoked hypersensitivity[35,36]. In contrast to our nocebo paradigms, CCK antagonism failed to attenuate threat-evoked hypersensitivity (Supplementary Fig. 11b), avoidance (Supplementary Fig. 11c, d), unconditioned freezing to the threat stimulus (Supplementary Fig. 11e), or conditioned freezing upon re-exposure to the threat-paired context (Supplementary Fig. 11f). This suggests that CCK signaling is not required for innate defensive responses but is necessary for expectancy-dependent amplification of pain.

CCK receptors mediate nocebo hyperalgesia within the lateral periaqueductal gray

For these next experiments, we aimed to demonstrate that activation patterns in the PAG were not specific to any model but rather indicative of the broader nocebo effect. Thus, we used the conditioned pain (i.e., hind paw incision as the UCS) and social pain observation assays to characterize active (i.e., c-Fos-positive) neurons within the PAG (Fig. 2a, b). A survey of the PAG along its rostral-caudal axis (Fig. 2c) revealed similar c-Fos-positive activation patterns in the contextual and the social nocebo assays. Specifically, the contextual and social nocebo assays showed no change in the precommisural nucleus (Prc), which is the most anterior portion of the PAG (aPAG, Fig. 2d). However, within the intermediate portion (imPAG; bregma −3.6 to −3.9 mm) of the nucleus, we observed increased c-Fos-positive neurons in the dorsomedial (dmPAG), dorsolateral (dlPAG) and lateral (lPAG) columns of mice returned to the same context (contextual nocebo) and in PO mice (social nocebo) (Fig. 2e), which was blocked by pre-treatment with proglumide in both paradigms. No apparent difference between the conditions for either assay was observed in the posterior PAG (pPAG; bregma −4.7 to −4.9 mm) in any of the columns (Fig. 2f). Representative images for c-Fos staining are shown for the imPAG for contextual and social nocebo in Fig. 2g, h, respectively.

Next, we sought to determine whether CCK receptors in the intermediate dmPAG or lPAG were critical for nocebo pain behavior in mice. To do this, we cannulated mice in both regions and tested whether application of proglumide interfered with contextual or social nocebo pain. We also infused CCK-8S into these regions to assess whether activation of CCK receptors was sufficient to evoke pain behavior. The intermediate dmPAG was selected due to its well-established role in sustained fear and anxiety states[37,38], while the lPAG was chosen for its involvement in social behavior[39] and pain processing[40]—both of which are highly relevant to nocebo pain behavior. Although we observed increased c-Fos-positive cells in the dlPAG of our nocebo groups, this region is largely associated with active defensive behaviors[41], such as escape, which are less relevant to nociceptive processing of social stimuli. Mice infused with proglumide into the intermediate dmPAG continued to show enhanced pain behavior in the contextual and social nocebo models (Fig. 3a–c), while CCK-8S infusion in the intermediate dmPAG did not increase sensitivity to mechanical stimulation (Fig. 3d) or responses on the hot plate test (Fig. 3e). In contrast, proglumide infusion into the intermediate lPAG blocked pain hypersensitivity in both models (Fig. 3f–h). Importantly, neither systemic proglumide (Supplementary Fig. 12a, b) nor intra-lPAG proglumide (Supplementary Fig. 12c) altered baseline nociceptive responses or acute injury-evoked pain in the absence of nocebo conditioning. Application of proglumide to the intermediate lPAG also did not affect distance traveled or velocity in an open field test (Supplementary Fig. 13a, b), indicating that the effects of proglumide on nocebo pain were not simply attributable to altered motor behavior. However, unlike the intermediate dmPAG, CCK-8S microinfusion into the intermediate lPAG increased mechanical sensitivity (Fig. 3i) and pain behavior on the hot plate test (Fig. 3j) and radiant heat paw-withdrawal test (Supplementary Fig. 14). Differences in drug spread were unlikely to account for our results, as fluorescent muscimol infusions revealed comparable spread within the dmPAG (Supplementary Fig. 15a) and lPAG (Supplementary Fig. 15b) with minimal crossover between PAG columns.

Finally, we asked whether neurons activated during nocebo preferentially expressed the CCK-2 receptor. The CCK-2 receptor, encoded by *Cckbr*, is the predominant CCK receptor subtype in the brain[42] and is expressed at high levels in the PAG[43]. Using RNAscope, we quantified *Cckbr* transcript abundance in Fos-positive neurons within the lPAG following both contextual and social nocebo paradigms. In the contextual nocebo paradigm, re-exposure to the pain-paired environment increased *Fos* expression in the lPAG, with a higher proportion of activated neurons expressing *Cckbr* compared with mice tested in a different context (Fig. 4a, b). Binning Fos^+ neurons by *Cckbr* RNAscope transcript abundance showed that this increase was driven primarily by recruitment of neurons expressing low-to-moderate levels

https://doi.org/10.1038/s41467-026-73266-y

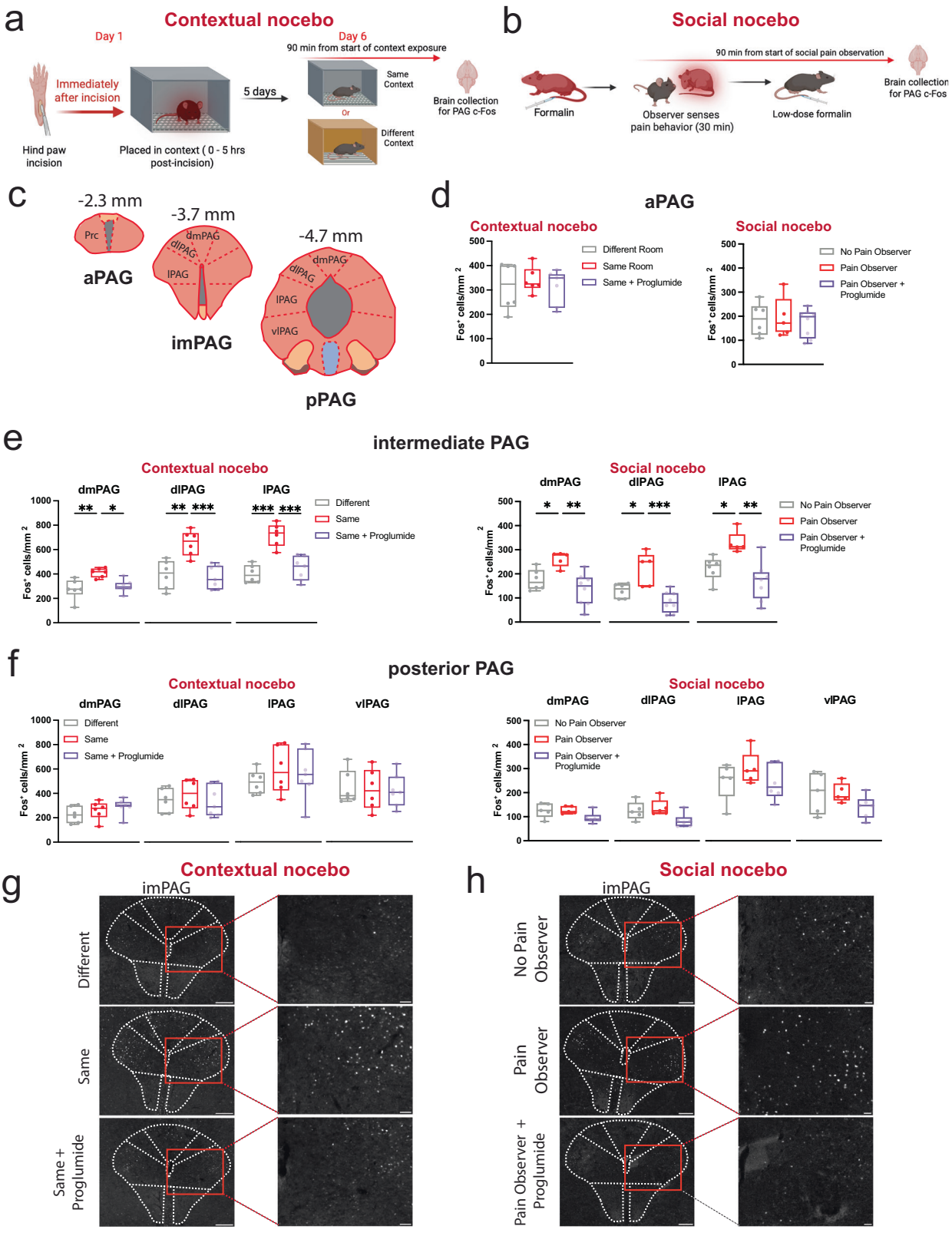

of *Cckbr* transcripts (Fig. 4c). A similar pattern was observed in the social nocebo paradigm, where PO mice exhibited increased *Fos* expression in the lPAG with co-localization of *Cckbr* transcripts, along with a higher fraction of *Fos*$^+$ neurons expressing *Cckbr* relative to NPO control mice (Fig. 4d, e). In contrast to the contextual model, transcript binning in the social paradigm indicated that the increase in *Cckbr* colocalization was driven primarily by *Fos*$^+$ neurons in the highest *Cckbr* abundance bin (15+ puncta), rather than by low-to-moderate expressing cells (Fig. 4f).

To further define the molecular identity of *Cckbr*-expressing neurons in the PAG, we analyzed spatial transcriptomic data from the Allen Brain Cell Atlas[44]. *Cckbr* expression in the PAG was largely confined to a small subset of glutamatergic neurons, representing ~4% of the glutamatergic population, with minimal expression in GABAergic

https://doi.org/10.1038/s41467-026-73266-y

Fig. 2 | Activation of periaqueductal gray (PAG) subregions by contextual and social nocebo pain in male mice. Timelines of contextual nocebo (**a**) and social nocebo (**b**) pain models used to capture neuronal activation via c-Fos immunohistochemistry. Created in BioRender. Martin, L. (2026) https://BioRender.com/q45b322 and https://BioRender.com/n29o201, respectively. **c** Schematic of the PAG showing bregma levels used for c-Fos quantification, across anterior (aPAG), intermediate (imPAG), and posterior (pPAG) divisions. Quantification of c-Fos-positive cells in the aPAG (**d**), imPAG (**e**), and pPAG (**f**) following contextual and social nocebo paradigms. Representative photomicrographs of the imPAG from contextual (**g**) and social (**h**) nocebo groups. Scale bars, **g** 200 μm and 50 μm; **h** 160 μm and 30 μm. Contextual: different ($n = 6$ mice), same ($n = 6$ mice), same + Prog. ($n = 7$ mice). Social (no pain observers, NPO; pain observers, PO) sample sizes varied by PAG subregion (NPO/PO/PO + Prog.): aPAG, 6/5/8 mice; imPAG, 6/5/8 mice; pPAG, 5/5/6 mice. Box plots show the median and interquartile range, with dots representing average c-Fos counts per mm^2 across three sections per mouse at each bregma coordinate. Columns of PAG quantification include dorsomedial, dorsolateral, lateral PAG, and ventrolateral (dmPAG, dlPAG, lPAG, and vlPAG, respectively). Statistical analyses were performed using one-way ANOVA for each PAG column to compare groups within the contextual and social nocebo conditions. $^*p < 0.05$, $^{**}p < 0.01$, and $^{***}p < 0.001$ from Šidák-corrected post hoc comparisons. Exact p values: **e** Contextual nocebo: dmPAG: 0.0035 (different vs. same) and 0.0121 (same vs. same + Prog.); dlPAG: 0.0016 (different vs. same) and 0.0006 (same vs. same + Prog.); lPAG: 0.00004 (different vs. same) and 0.00013 (same vs. same + Prog.). Social nocebo: dmPAG: 0.037 (NPO vs. PO) and 0.0018 (PO vs. PO + Prog.); dlPAG: 0.017 (NPO vs. PO) and 0.0004 (PO vs. PO + Prog.); lPAG: 0.035 (NPO vs. PO) and 0.0011 (PO vs. PO + Prog.). Full statistical reporting is provided in Supplementary Data 1. Source data are provided as a Source data file.

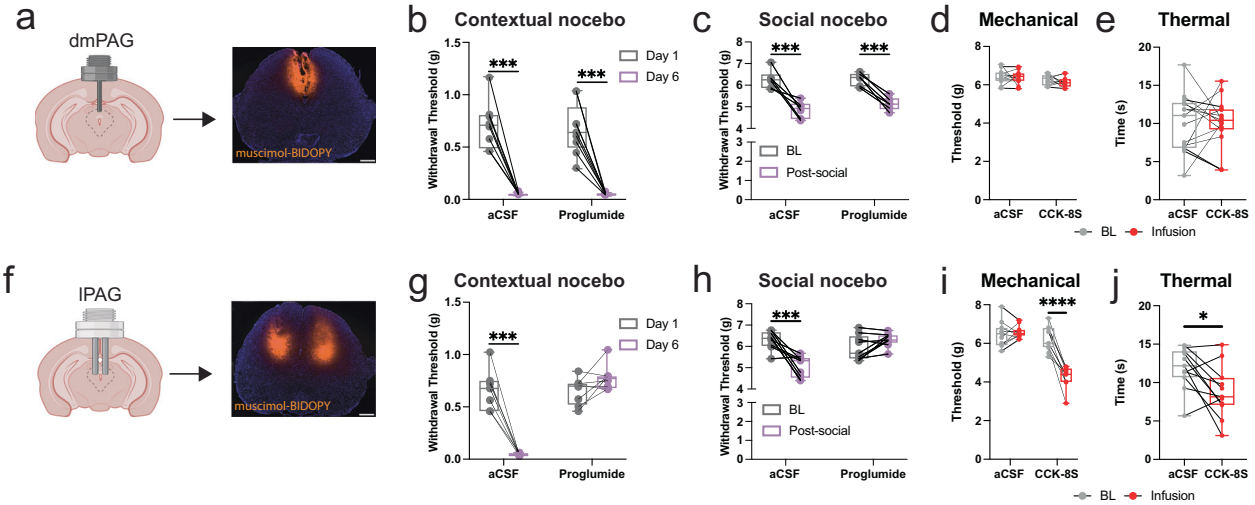

Fig. 3 | Activation of cholecystokinin receptors in the lateral, but not dorsomedial, periaqueductal gray is required for nocebo-induced pain and sufficient to elicit pain-related behavior. a Schematic and representative micrograph illustrating cannulation targeting the intermediate dorsomedial periaqueductal gray (dmPAG). Created in BioRender. Martin, L. (2026) https://BioRender.com/y1pi5q0. Fluorescent muscimol was used to visualize injection spread. Scale bar, 100 μm. Intra-dmPAG infusion of proglumide does not alter contextual (**b** $n = 8$ mice per group, 4 M, 4 F) or social nocebo responses (**c** $n = 6$ mice per group, 3 M, 3 F). Intra-dmPAG infusion of CCK-8S does not affect mechanical thresholds (**d** $n = 11$ mice per group, 5 M, 6 F) or hot plate latency (**e** $n = 15$ mice per group, 5 M, 10 F). **f** Schematic and representative micrograph illustrating cannulation targeting the intermediate lateral PAG (lPAG). Created in BioRender. Martin, L. (2026) https://BioRender.com/d97azz9. Fluorescent muscimol was used to visualize injection spread. Scale bar, 500 μm. Intra-lPAG infusion of proglumide attenuates contextual (**g** aCSF $n = 7$ mice, 3 M, 4 F; proglumide $n = 8$ mice, 3 M, 5 F) and social nocebo responses (**h** $n = 9$ mice per group, 4 M, 5 F). Intra-lPAG infusion of CCK-8S increases mechanical sensitivity (**i** $n = 11$ mice per group, 6 M, 5 F) and reduces hot plate latency (**j** $n = 11$ mice per group, 5 M, 6 F). Box plots show the median and interquartile range, with paired measurements from individual mice. Separate two-way ANOVAs (drug × time) were used for contextual (**b**, **g**) and social nocebo (**c**, **h**). Two-way mixed ANOVA was used for mechanical sensitivity (**d**, **i**), and paired two-sided t-tests for hot plate latency (**e**, **j**). $^{**}p < 0.01$, $^{***}p < 0.001$ from Šidák-corrected post hoc comparisons or Bonferroni corrected two-sided t-tests where appropriate. Exact p values: **b** 2.42×10^{-9} (aCSF) and 5.45×10^{-9} (proglumide); **c** 0.0001 (aCSF) and 0.0004 (proglumide); **g** 3.81×10^{-5}; **h** 0.00013; **i** 2.14×10^{-9}; **j** 0.0012. Full statistical reporting is provided in Supplementary Data 1. Source data are provided as a Source data file.

cells (Supplementary Fig. 16a). *Cckbr*$^+$ glutamatergic neurons showed extensive co-expression with the μ-opioid receptor gene (*Oprm1)* and the cannabinoid receptor 1 gene (*Cnr1),* with ~50% expressing both genes within the same cell. In contrast, overlap with stress-related markers, such as *Crh* and *Crhr1* was rare (Supplementary Fig. 16b). Spatial mapping showed that *Cckbr*$^+$ glutamatergic neurons were distributed across dorsal and lateral regions of the PAG, with *Pou4f1*-associated lineages enriched in the lPAG at intermediate and posterior levels (Supplementary Fig. 16c). Quantification across the rostral-caudal axis of the PAG confirmed that *Pou4f1*-derived neurons were most abundant at intermediate levels of the PAG (Supplementary Fig. 16d). Further, *Cckbr*$^+$ *Pou4f1* neurons showed prominent co-expression of *Oprm1* and *Cnr1*, positioning this population to modulate descending pain control through established opioid- and endocannabinoid-sensitive PAG circuits (Supplementary Fig. 16e).

Identification of long-range CCK projections that mediate nocebo behavior

To determine whether the source of CCK within the lPAG arises from projection neurons in other brain regions, we infused a Cre-dependent retrograde AAV expressing mNeptune into the intermediate lPAG of CCK-IRES-Cre mice (Fig. 5a–c). Retrogradely labeled neurons were detected in several cortical regions, including the insula, motor cortex, retrosplenial cortex, and parietal cortex (Fig. 5b–d). However, we identified a distinct and densely labeled population of CCK projection neurons in the anterior cingulate cortex (ACC) (Fig. 5b–e). These ACC neurons were largely confined to layer V and constituted the most prominent source of CCK-positive projections to the intermediate lPAG (Fig. 5e). Quantification across regions confirmed that the ACC showed a significantly higher proportion of retrogradely labeled CCK$^+$ neurons relative to total NeuN-positive cells compared to all other regions examined (Fig. 5f). Immunocytochemical analysis revealed

https://doi.org/10.1038/s41467-026-73266-y

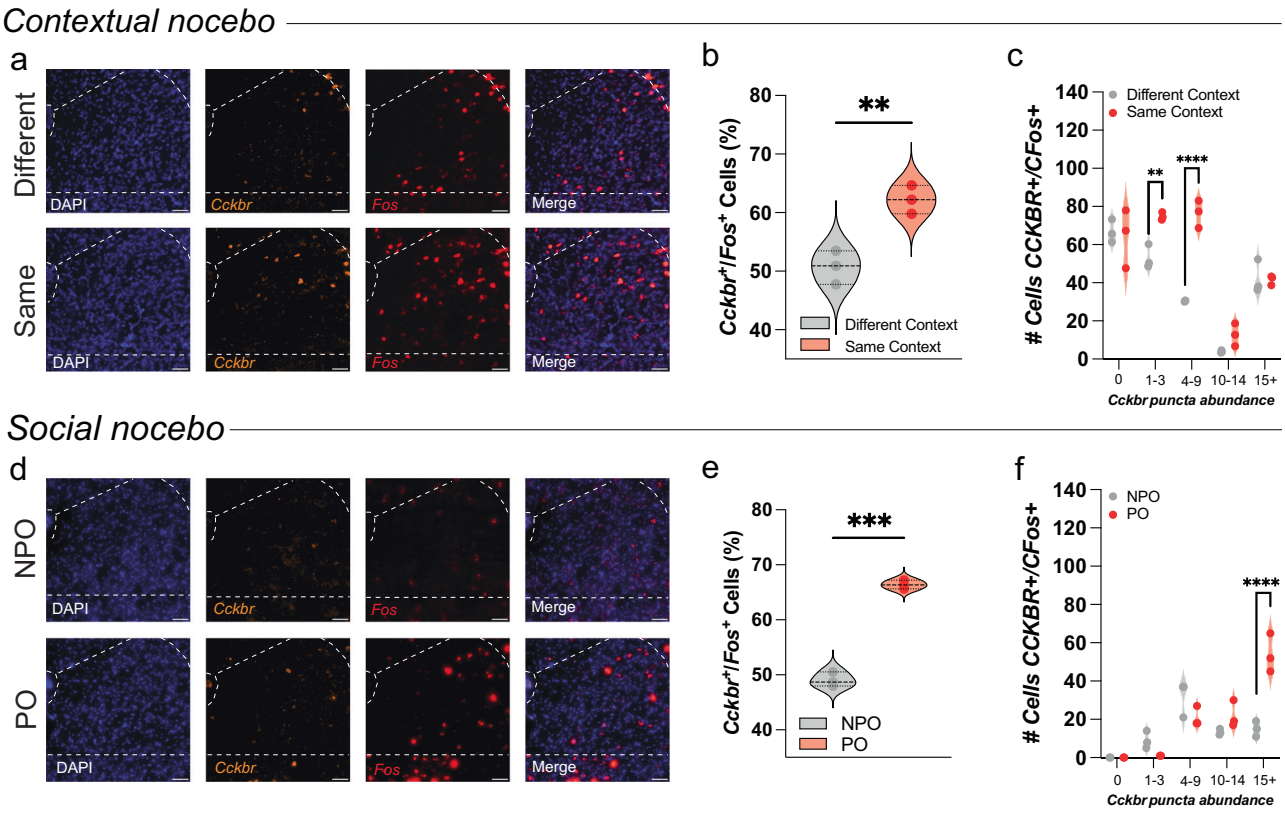

Fig. 4 | *Cckbr*-expressing neurons in the lateral periaqueductal gray (lPAG) are recruited during contextual and social nocebo. a Representative RNAscope image showing *Fos* expression in neurons that contain *Cckbr* mRNA within the intermediate lPAG of mice re-exposed to the same or a different context. Scale bar, 100 μm. **b** Violin plots showing quantification of *Cckbr*$^+$/*Fos*$^+$ neurons in the lPAG of mice re-exposed to the same or a different context ($n = 3$ male mice per group; 3 slices per mouse). **c** Violin plots showing the number of *Fos*$^+$ neurons in the lPAG expressing increasing *Cckbr* transcript levels, binned by puncta abundance (0, 1–3, 4–9, 10–14, 15+ per cell), in mice re-exposed to the same or a different context. **d** Representative RNAscope images showing *Fos* expression in neurons that contain *Cckbr* mRNA within the intermediate lPAG following social nocebo. Scale bar, 100 μm. **e** Violin plots showing quantification of *Cckbr*$^+$/*Fos*$^+$ neurons in the lPAG of no pain observers (NPO; 3 mice per group; 3 slices per mouse, 1 M, 2 F) or pain observers (PO; 3 mice per group; 3 slices per mouse, 1 M, 2 F). **f** Violin plots showing the number of *Fos*$^+$ neurons in the lPAG expressing increasing *Cckbr* transcript levels, binned by puncta abundance (0, 1–3, 4–9, 10–14, 15+ per cell), in NPO versus PO mice following the social nocebo paradigm. Statistical tests used unpaired two-sided t-tests for **b**, **e** and two-way mixed ANOVAs (condition × puncta group) for (**c**, **f**). $^{**}p < 0.01$, $^{***}p < 0.001$ from Šidák-corrected post hoc comparisons or Bonferroni-corrected two-sided t-tests where appropriate. Exact *p* values: **b** 0.006; **c** 0.0057 (1–3) and 5.48×10^{-7} (4–9); **e** 4.18×10^{-5}; **f** 1.65×10^{-7}. Full statistical reporting is provided in Supplementary Data 1. Source data are provided as a Source data file.

that retrogradely labeled ACC^{CCK} neurons co-express EMX1 and exhibit pyramidal morphology, consistent with an excitatory phenotype (Supplementary Fig. 17). This is in line with transcriptomic classification of CCK-expressing ACC neurons (Supplementary Fig. 18).

To provide supporting evidence for involvement of the ACC^{CCK} → lPAG pathway during nocebo retrieval, we quantified c-Fos expression in retrogradely labeled neurons from a small subset of mice following re-exposure to the same or different context (Supplementary Fig. 19a). Consistent with behavioral reinstatement, context-dependent increases in overall c-Fos expression were observed selectively in the ACC layer 2/3, while enhanced c-Fos co-labeling in retrogradely labeled neurons was observed in ACC layer 5, specifically in the same-context condition (Supplementary Fig. 19b, c). No context-dependent differences in c-Fos or co-labeling with retrogradely labeled neurons were detected in other regions or layers (Supplementary Fig. 19d–f). To directly test whether ACC^{CCK} neurons were required for nocebo behavior, we next used a chemogenetic approach to silence CCK$^+$ neurons in the ACC during nocebo retrieval. Inhibition of ACC^{CCK} neurons selectively blocked contextual nocebo responses (Fig. 5g), whereas broader inhibition of excitatory CaMKIIa-expressing neurons in the ACC disrupted social nocebo responses (Fig. 5h), demonstrating a causal role for ACC^{CCK} and excitatory neurons in mediating nocebo pain behavior.

ACC^{CCK} → lPAG projections are critical for nocebo pain behavior and pain sensitivity

Based on the microinfusion and viral tracing experiments, we hypothesized that ACC^{CCK} neurons project to the lPAG to mediate nocebo pain behavior in mice. To test this, we targeted ACC^{CCK} terminals in the lPAG using projection-specific optogenetic inhibition. We injected an inhibitory opsin (eOPN3) into the ACC and implanted an optic cannula above the lPAG (Fig. 6a). After 3 weeks of expression, we tested whether optogenetically silencing ACC^{CCK} → lPAG projections disrupted contextual or social nocebo responses. During re-exposure to the pain-paired context, mice expressing a control virus displayed nocebo hypersensitivity, whereas optogenetic inhibition of ACC^{CCK} → lPAG terminals blocked contextual nocebo (Fig. 6b). A similar effect was observed in the social nocebo paradigm, where silencing this projection during pain observation prevented the expression of social nocebo (Fig. 6c). We next examined whether ACC^{CCK} → lPAG activity was required for contextual nocebo learning. Optogenetic inhibition of this pathway prior to conditioning did not alter baseline mechanical thresholds, and inhibition during the 5-h conditioning period likewise failed to prevent contextual nocebo hypersensitivity when mice were tested without optogenetic inhibition on day 6 (Fig. 6d). This suggests that suppressing ACC^{CCK} → lPAG signaling during baseline or conditioning was not sufficient to disrupt subsequent nocebo expression.

https://doi.org/10.1038/s41467-026-73266-y

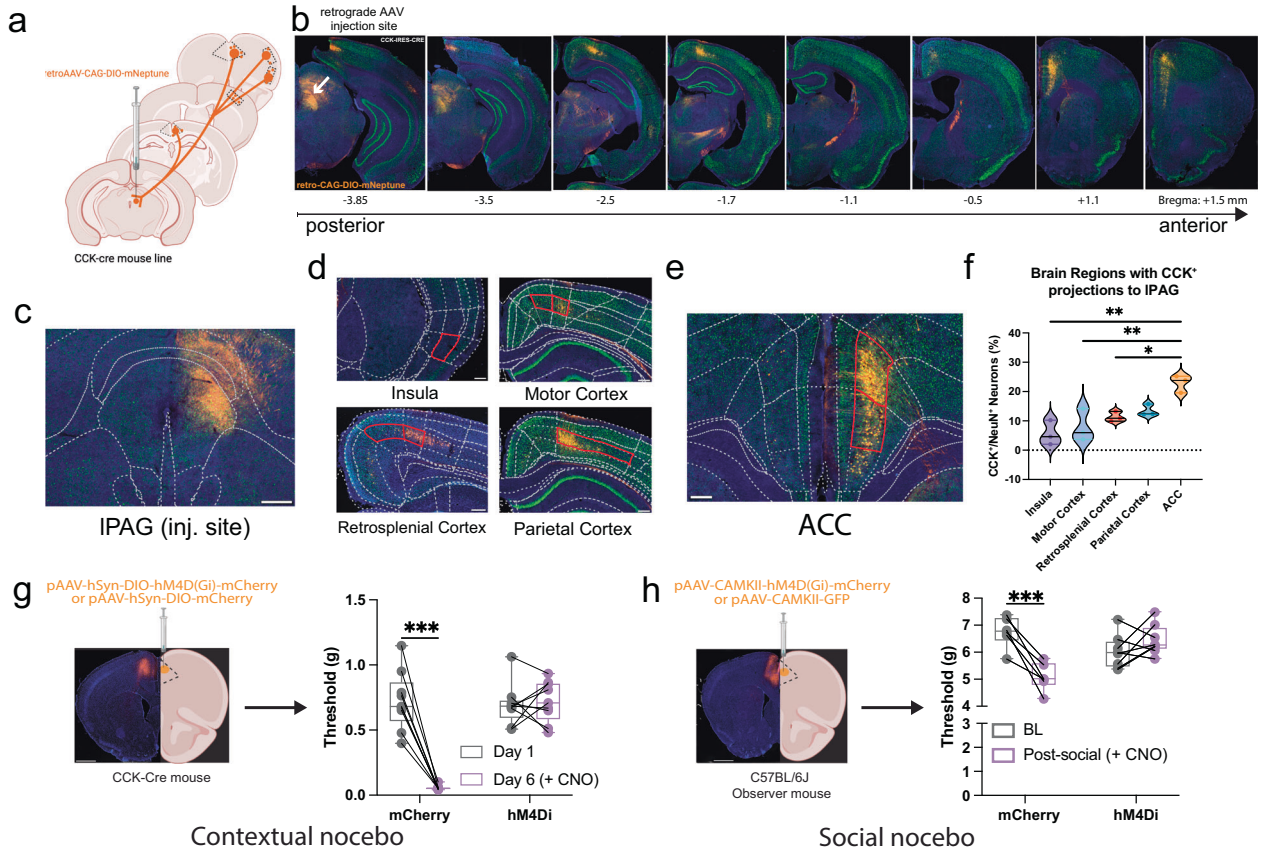

Fig. 5 | Cholecystokinin-expressing neurons in the anterior cingulate cortex (ACC) project to the lateral periaqueductal gray (lPAG) and are required for contextual and social nocebo-induced pain hypersensitivity. a Schematic illustrating Cre-dependent retrograde viral tracing from the intermediate lPAG using retroAAV-CAG-DIO-mNeptune in CCK-Cre mice ($n = 3$ male mice). Created in BioRender. Martin, L. (2026) https://BioRender.com/dtqi40y. **b** Representative sections showing retrogradely labeled CCK$^+$ projection neurons following lPAG injection. **c** Representative section of the lPAG injection site showing co-localization of retrograde mNeptune signal with NeuN. **d**, **e** Representative micrographs of the ACC showing retrograde labeling and co-localization with NeuN. NeuN$^+$ and NeuN$^+$/CCK$^+$ neurons were quantified within layer V. Scale bar, 200 μm. **f** Percentage of CCK$^+$ neurons relative to total NeuN$^+$ neurons in cortical regions projecting to the lPAG. **g** Chemogenetic inhibition of CCK$^+$ neurons using pAAV-hSyn-DIO-hM4D(Gi)-mCherry ($n = 9$ mice, 5 M, 4 F) or control virus ($n = 9$ mice, 4 M, 5 F) in CCK-Cre mice during contextual nocebo. Mechanical thresholds were measured before and after contextual re-exposure. **h** Chemogenetic inhibition of cortical excitatory neurons using pAAV-CaMKIIa-hM4D(Gi)-mCherry ($n = 8$ mice, 5 M, 3 F) or control virus ($n = 6$ mice, 3 M, 3 F) in C57BL/6 observer mice during social nocebo. Mechanical thresholds were measured at baseline and following pain observation. Violin plots (**f**) and box plots (**g**, **h**) show the median and interquartile range with individual mice overlaid. One-way ANOVA (**f**) and two-way ANOVAs (virus × time) were used for contextual and social nocebo experiments (**g**, **h**). $^*p < 0.05$, $^{**}p < 0.01$, and $^{***}p < 0.001$ from Šidák-corrected post hoc comparisons. Exact p values: **f** 0.0015 (ACC vs. insula), 0.0045 (ACC vs. motor cortex), and 0.026 (ACC vs. retrosplenial cortex); **g** 8.16×10^{-10}; **h** 7.05×10^{-10}. **g**, **h** Created in BioRender. Martin, L. (2026) https://BioRender.com/zsb8l03. Full statistical reporting is provided in Supplementary Data 1. Experiments in (**b**–**e**) were repeated independently three times with similar results. Source data are provided as a Source data file.

Because we showed that the ACC^{CCK} → lPAG pathway was necessary for contextual and social nocebo, we further aimed to determine whether its activation was sufficient to drive pain-like behavior. To this end, we expressed channelrhodopsin-2 (ChR2) coupled to a mCherry tag in CCK neurons of the ACC and implanted an optical fiber above the lPAG (Fig. 6e), with mCherry-only mice serving as controls. Optical stimulation of ACC^{CCK} → lPAG terminals with blue laser light (470 nm, 20 Hz, 10 mW/mm^2) produced marked mechanical hypersensitivity in ChR2-expressing mice, but not controls (Fig. 6f). This hypersensitivity emerged rapidly and persisted for approximately 60 min (Fig. 6g), indicating that activation of this projection was sufficient to induce a pain-like state. Finally, administration of the CCK receptor antagonist proglumide attenuated the hypersensitivity evoked by ACC^{CCK} → lPAG optogenetic stimulation (Fig. 6h).

Discussion

Here, we identify a cortico–midbrain circuit in which CCK released from ACC neurons activates CCK-2 receptors in the intermediate lPAG to amplify pain sensitivity under conditions of negative expectation. Across two distinct nocebo paradigms, we find convergent behavioral, pharmacological, anatomical, and circuit-specific evidence that this ACC^{CCK} → lPAG pathway is both necessary and sufficient for nocebo-like hyperalgesia in mice. The rigor and generalizability of our findings are enhanced by the independent but converging early work by two different laboratories, unaware of each other's findings.

In humans, proglumide attenuates nocebo hyperalgesia[10,11], and here both nonselective CCK receptor blockade and selective CCK-2 receptor antagonism prevented nocebo hypersensitivity. This effect cannot be explained by a general reduction in nociception or stress responses, as systemic proglumide left baseline sensitivity and formalin-evoked behavior unchanged, and intra-lPAG proglumide did not affect incision-evoked pain outside of the nocebo context. Likewise, a predator-odor paradigm that produces robust stress-evoked hypersensitivity and avoidance[36,45] remained intact under proglumide, indicating that CCK signaling is not required for general stress-induced hyperalgesia and defensive responses induced by this stimulus. This

https://doi.org/10.1038/s41467-026-73266-y

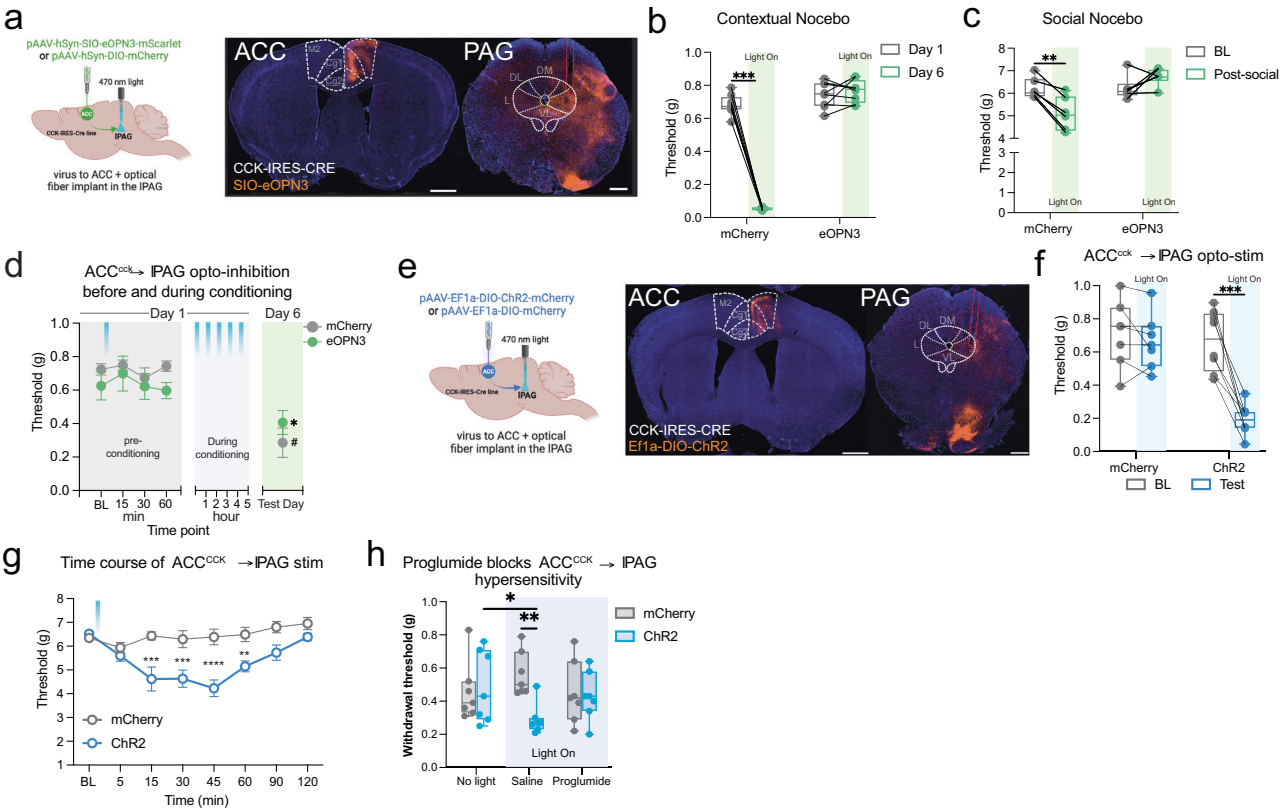

Fig. 6 | Cholecystokinin-expressing anterior cingulate cortex (ACC) neurons projecting to the lateral periaqueductal gray (lPAG) are required for nocebo-induced pain hypersensitivity and sufficient to drive pain behavior. **a** Experimental schematic illustrating targeting of ACC^{CCK} → lPAG projections using eOPN3 or mCherry. Created in BioRender. Martin, L. (2026) https://BioRender.com/y9tttu0. Representative sections showing ACC expression and PAG terminals. Mechanical withdrawal thresholds measured before and after contextual re-exposure (**b** $n = 8$ mice per group, 5 M, 3 F) or pain observation (**c** $n = 6$ mice per group, 3 M, 3 F) during optogenetic inhibition of ACC^{CCK} → lPAG projections (light on). **d** Time course of mechanical thresholds during contextual conditioning, with inhibition of ACC^{CCK} → lPAG projections during conditioning ($n = 9$ mCherry mice, 6 M, 3 F; $n = 6$ eOPN3 mice, 2 M, 4 F). **e** Experimental schematic illustrating targeting of ACC^{CCK} → lPAG projections using ChR2 or mCherry. Created in BioRender. Martin, L. (2026) https://BioRender.com/bizkjrb. Representative sections showing ACC expression and PAG terminals. **f** Optogenetic activation of ACC^{CCK} → lPAG projections induces mechanical hypersensitivity in ChR2-expressing mice ($n = 8$ mice, 4 M, 4 F) but not in mCherry controls ($n = 7$ mice, 3 M, 4 F). **g** Time course of mechanical thresholds during optogenetic activation of ACC^{CCK} → lPAG projections ($n = 7$ mice per group, 4 M, 3 F for mCherry; 3 M, 4 F for ChR2). **h** Intra-lPAG infusion of proglumide attenuates optogenetically evoked hypersensitivity during ACC^{CCK} → lPAG stimulation ($n = 7$ mice per group, 4 M, 3 F for mCherry; 3 M, 4 F for ChR2). Box plots show the median and interquartile range with paired measurements from individual mice. Data in (**d**, **g**, **h**) are shown as mean ± SEM. Two-way mixed ANOVAs (virus × time) were used for (**b**–**d**, **f**–**h**). $^{*}p < 0.05$, $^{**}p < 0.01$, and $^{***}p < 0.001$ from Šidák- or Tukey-corrected post hoc comparisons where appropriate. In **d** $\#p < 0.05$ compared with ChR2 no-light baseline; $^{*}p < 0.05$ compared with mCherry no-light baseline. Exact p values: **b** 1.81×10^{-12}; **c** 0.0044; **d** 0.013 (mCherry) and 0.048 (eOPN3); **f** 1.59×10^{-6}; **g** 1.48×10^{-4} (15 min), 6.08×10^{-4} (30 min), 4.59×10^{-6} (45 min), and 0.0096 (60 min). **h** 0.0039 (saline light on, mCherry vs. ChR2) and 0.039 (no light vs. light on, ChR2 only). Full statistical reporting is provided in Supplementary Data 1. Source data are provided as a Source data file.

aligns with human findings that proglumide reduces nocebo hyperalgesia while leaving the associated endocrine stress response unchanged[46], demonstrating that CCK blockade uncouples pain amplification from stress physiology rather than directly suppressing the stress response. This contrasts with conditions of intense or sustained stress, where social defeat produces widespread increases in brain CCK and engages endocrine responses, and chronic treatment with the selective CCK-2 antagonist CI-988 reduces corticosterone elevation[47] and stress-enhanced formalin pain[48]. Such effects likely reflect large-scale recruitment of CCK during sustained threat, whereas our paradigms depend on CCK signaling within a defined cortical–PAG circuit. This suggests that CCK recruitment depends on the nature of the threat signal, supporting a model in which CCK is not universally engaged by pain or stress, but can be selectively recruited to amplify nociceptive processing under conditions of negative expectation.

Our dataset provides an analysis of the PAG across coronal planes and along the anterior-posterior axis, revealing distinct PAG columns activated by our nocebo paradigms, extending beyond the typically studied posterior PAG. The contextual and social nocebo paradigms increased c-Fos expression in the intermediate lPAG, an effect blocked by proglumide, identifying this region as a crucial hub for CCK-dependent nocebo pain responses. This mirrors human fMRI findings localizing nocebo responses to more rostral lateral PAG regions than placebo responses[26]. Although evidence from animal models in support of the role of the PAG in nocebo hyperalgesia has been limited, our findings, coupled with recent studies of conditioned and socially enhanced nausea behaviors in rats[49], highlight the significance of the PAG and its interconnected regions, such as the ACC, in nocebo effects. At the cellular level, the contextual nocebo paradigm recruited a broader population of Fos-positive lPAG neurons expressing predominantly low-to-moderate levels of *Cckbr* transcripts, whereas the social nocebo condition engaged fewer neurons but was enriched for cells with high *Cckbr* expression, indicating recruitment of distinct gain states within the same circuit rather than uniform scaling of activity. At intermediate rostral-caudal levels of the PAG, *Cckbr*$^{+}$ neurons were enriched within a population marked by expression of *Pou4f1*, a transcription factor associated with defined neuronal lineages in sensory systems[50,51]. Although *Pou4f1* has not been directly linked to

descending pain modulation, its enrichment within specific *Cckbr*$^{+}$ PAG neurons, together with co-expression of *Oprm1* and *Cnr1*, is consistent with engagement of circuits known to regulate nociceptive processing.

Previous work has established that glutamatergic ACC projections to the dlPAG and lPAG contribute to reflexive and active avoidance of pain[52], but it remains unclear whether these effects reflect broad engagement of ACC output or selective recruitment of defined neuronal populations under specific cognitive conditions. Our findings suggest that nocebo expression depends on selective engagement of a predominantly excitatory, CCK-expressing population of ACC neurons projecting to the intermediate lPAG. Although CCK is expressed in both excitatory and inhibitory cortical neurons[53], several observations indicate that the nocebo effect is largely mediated by an excitatory population. ACC^{CCK} → lPAG-projecting neurons were confined to layer V and displayed pyramidal morphology characteristic of corticofugal glutamatergic cells. Retrograde tracing combined with Fos mapping showed selective activation of these projection neurons during nocebo expression rather than broad activation of local cortical networks, and spatial transcriptomic classification further demonstrated that ACC^{CCK} expression is strongly enriched in intratelencephalic (IT)- and extratelencephalic (ET)-type excitatory subclasses, with interneurons representing only a minor fraction. Consistent with this, chemogenetic inhibition of ACC^{CCK} or ACC^{CaMKIIa} neurons, or optogenetic inactivation of ACC^{CCK} terminals in the lPAG blocked nocebo hypersensitivity. Conversely, optogenetic activation of the ACC^{CCK} → lPAG pathway was sufficient to induce mechanical allodynia, which was blocked by proglumide. These findings suggest that CCK release from ACC terminals acts as a gain-modulating signal that biases nociceptive output through enhanced glutamate release[54], consistent with anti-opioid and pain-facilitatory roles of CCK signaling[46,55,56]. Inhibition of the ACC^{CCK} → lPAG pathway during conditioning did not prevent subsequent nocebo expression, indicating that this pathway is recruited during expression rather than acquisition of contextual nocebo associations.

Placebo and nocebo effects are often viewed as mechanistically dissociable because they can engage distinctt neural and biochemical pathways. Placebo analgesia, for instance, can be disrupted by the opioid receptor antagonist, naloxone, demonstrating the involvement of endogenous opioids[57]. Conversely, in human models of nocebo hyperalgesia, increased pain responses are not reversed by naloxone[10]. Interestingly, application of the CCK-2 receptor agonist, pentagastrin, disrupts placebo analgesia in humans[58], whereas proglumide enhances placebo responses[11]. Recent circuit-level studies of placebo analgesia indicate that expectation engages a descending inhibitory pathway in which cortical signals recruit ventrolateral PAG neurons that project to the rostral ventromedial medulla and suppress nociceptive transmission through endogenous opioid signaling[8,59,60]. In these models, cortical input from medial prefrontal cortex (mPFC) and ACC gates activity of vlPAG projection neurons, producing analgesia only when expectations of pain-relief or lower pain are present rather than through nonspecific activation of the PAG. Positive expectation, therefore, preferentially engages opioid-dependent vlPAG output that suppresses nociceptive transmission, while negative expectation recruits a CCK-sensitive population in the intermediate lPAG that facilitates pain processing. Rather than activating separate modulatory pathways, expectation appears to bias a shared ACC–PAG circuit toward either inhibitory or facilitatory output.

Evidence of human pain as a learning phenomenon continues to grow[61–65], as does evidence for the social modulation of pain[62–65]. The prognosis of pain patients is worsened by sometimes inadvertent nocebo suggestions by clinical providers[66], and substantial psychological risk factors, such as anxiety, harm avoidance, and pain catastrophizing can be conceptualized as an auto-nocebo process[67]. However, nocebo effects are generally greater in female subjects[68], whereas we did not observe differences between male and female mice in our nocebo models. This discrepancy may reflect species differences in baseline anxiety levels, hormonal regulation, or variations in experimental paradigms. Addressing these factors through comparative studies involving additional species and human-like conditioning protocols will help clarify the observed differences and strengthen the translational applicability of our findings[62–65].

Our focus on CCK signaling was informed by prior human pharmacological studies implicating CCK in nocebo effects and expectancy-driven pain modulation. By isolating CCK-dependent signaling from the ACC to the lPAG as a key mechanism for nocebo hyperalgesia, our findings distinguish negative expectation-driven pain amplification from generalized stress or injury-related hypersensitivity. More broadly, the mouse models described here provide a controlled experimental approach for examining how contextual and social cues shape nociceptive processing, offering a basis for future studies of negative expectation-dependent modulation of pain.

Methods

Animals

Most experiments used naïve, adult CD-1 (ICR:Crl) or C57BL/6 mice aged 6–13 weeks. Both male and female mice were used; sex composition varied by experiment and is specified in the figure legends and Source data files. Sex was not included as a primary experimental factor unless otherwise stated. CD-1 mice were bred in-house at McGill University, originating from breeders obtained from Charles River (St. Constant, QC). C57BL/6 mice were obtained from Charles River (St. Constant, QC) and housed in the University of Toronto Mississauga vivarium for at least 2 weeks prior to behavioral testing, or were bred in-house from our established colony. Experiments targeting CCK neurons used offspring bred in-house (UTM) from CCK-IRES-Cre mice, which were originally purchased from The Jackson Laboratory (Bar Harbor, ME; Stock #012706). All mice were group-housed in cages of 2–4 on individually ventilated cage racks (Techniplast North America) in temperature-controlled rooms (22 ± 2 °C) under a 12:12 h light/dark cycle (lights on at 07:00 h) with access to food (Harlan Teklad 8604 for McGill mice; 2019 Teklad for UTM mice) and water ad libitum. Mice were randomly allocated to experimental groups, and testing was conducted by multiple female experimenters[69] who were blind to drug treatments. CCI-based conditioning experiments were conducted exclusively in CD-1 mice. Hind paw incision and extinction experiments were performed in CD-1 and C57BL/6 mice across two independent cohorts with similar results. Social nocebo paradigms and all tissue-based analyses were conducted in C57BL/6 mice. All procedures adhered to the Canadian Council on Animal Care guidelines. Experiments conducted at the University of Toronto were approved by the University of Toronto Animal Care Committee, and experiments conducted at McGill University were approved by the McGill University Animal Care Committee.

Contextual nocebo conditioning

The contextual nocebo conditioning paradigms comprised three distinct phases: baseline testing, where basal thresholds were measured, the learning session, during which the association between pain (unconditioned stimulus, UCS) and context (conditioned stimulus, CS) was formed, and the testing day, which assessed the response to the presentation of the CS. Two different pain stimuli were used as the UCSs: hind paw incision or chronic constriction injury, as described below. Prior to surgery, mechanical thresholds were assessed using the von Frey test (see below). On the learning day, mice underwent either hind paw incision surgery on their left paw to induce post-surgical pain, or chronic constriction injury (CCI) on their left leg, which served as the UCSs. Following surgery, while still under anesthesia, the mice were placed in the conditioning context, consisting of Plexiglas cubicles within a specific laboratory testing room, where they remained for 5 h, most of which was spent awake. Mice subjected to incision and CCI

surgery were returned to the same or different context at 6 or 14 days after surgery, respectively. On test days, mice were retested for pain sensitivity following a 10–90-min habituation period using the manual von Frey test. For baseline and test day measurements, four separate determinations, two per hind paw, were conducted and averaged.

Social nocebo paradigm

Same-sex cagemate pairs were placed in an open top/bottom box (inner dimensions: 14.5 cm × 14.5 cm × 30 cm) with three opaque sides and one clear side. Each box was set on top of a clear acrylic platform, which was either placed on a frame for video recording from below during the formalin assay or set on top of a laboratory bench for all other assays. For each experiment, pairs of mice were habituated to the box for 1 h. Mice in the pair were randomly assigned as either observer or demonstrator. Following habituation, the demonstrator was removed briefly, administered an intraplantar hind paw injection of formalin (2.5%, 20 µl; pain observer condition), or saline (0.09%) as a no-pain control stimulus (no pain observer condition). Formalin hind paw injection was selected as the pain stimulus due to the characteristic pattern of overt nocifensive behaviors that are reliably perceived by observer mice[15,70]. The observer and demonstrator were then allowed to interact for 30 min, consistent with previous social transfer models[14,15,31,70]. Following the 30 min one-in-pain social interaction, the demonstrator was removed from the box and returned to its home cage. The observer was then either tested for formalin sensitivity (0.5%, 20 µl, intraplantar) or placed in individual Plexiglas cubicles over a metal mesh platform for electronic von Frey testing (see below). For von Frey testing, baseline measurements consisted of five separate determinations for each hind paw, which were averaged. In most experiments, mechanical sensitivity was assessed beginning 10 min after placement in the Plexiglas cubicle, and values represent the average of two measurements per paw.

Predator threat-evoked hypersensitivity paradigm

To assess whether CCK signaling contributes to unconditioned stress-evoked pain modulation, mice underwent a single-exposure predator odor conditioning procedure using trimethylthiazoline (TMT, 10%). Baseline mechanical sensitivity was first measured using manual von Frey testing. Twenty-four hours later, mice were allowed 5 min of free exploration in a two-chamber apparatus to determine side preference. After an additional 24 h, mice received proglumide (10 mg/kg) or saline 30 min before conditioning. They were first placed in the non-preferred chamber for a 5-min neutral exposure and, 2 h later, exposed for 5 min to filter paper containing 10% TMT. Mechanical sensitivity was reassessed 3 h after TMT using the von Frey test. Contextual memory and defensive behavior were subsequently evaluated using a conditioned place aversion procedure, followed 24 h later by a 5-min preference test. Manual von Frey thresholds were then measured across the following 21 days. Ten days after the conditioned place aversion test, conditioned freezing was quantified during 5-min re-exposures to both the unpaired and TMT-paired chambers. This delayed assessment was included because we previously demonstrated that blocking corticosterone synthesis prior to initial TMT exposure prevents both unconditioned freezing to TMT and conditioned freezing to the TMT-paired context when mice were returned 10 days later[36]. The TMT paradigm differs from contextual nocebo conditioning in that hypersensitivity is triggered by an unconditioned threat rather than a learned pain-predictive association.

von Frey test

Testing of mechanical sensitivity was performed using either the manual or electronic von Frey test. Manual von Frey: In contextual nocebo experiments, mice were placed individually in transparent Plexiglas cubicles (5 cm × 8.5 cm × 6 cm) on top of a perforated metal floor and habituated for 2 h before testing. Nylon monofilaments (force range: ≈0.015 to 1.3 g; touch test sensory evaluator kit, Stoelting) were firmly applied to the plantar surface of each hind paw of an inactive mouse until they bowed for 0.5 s. The up-down method of Dixon[71] was used to estimate 50% withdrawal thresholds. Electronic von Frey: In social nocebo experiments, observers were placed in individual Plexiglas cubicles (10 cm × 5.5 cm × 6.5 cm) over a metal mesh platform and allowed to habituate for 30 min prior to baseline testing. Mice were tested using a dynamic plantar aesthesiometer (Ugo Basile, 37450, Gemonia, Italy), which raised a blunt 0.5-mm metal probe onto the center of the hind paw and gradually applied force (0–10 g ramp over 10 s) until the mouse withdrew its hind paw. The maximal pressure displayed upon withdrawal was recorded.

Radiant heat paw-withdrawal test

The radiant heat paw-withdrawal test was used to assess acute thermal nociception sensitivity in mice[72]. Prior to behavioral testing, mice were individually housed in perforated, transparent Plexiglas enclosures (5 cm × 8.5 cm × 6 cm) situated on a glass floor with a thickness of 3/16th inches and allowed to acclimate for 2 h. A high-intensity beam (IITC model 336; ≈45 W) emitted from a projector lamp bulb positioned 6 cm beneath the glass floor was directed at the plantar surface of the mid-hind paw of each mouse at rest. Withdrawal latency of each hind paw was recorded to the nearest 0.1 s.

Formalin test

In social nocebo experiments, chemical pain sensitivity in observer mice was assessed using a low concentration formalin challenge (0.5%, 20 µl, intraplantar injection into the left hind paw). This concentration was chosen because it elicits minimal nocifensive behavior while avoiding behavioral ceiling effects that are typically observed at higher concentrations[73]. Following injection, observer mice were returned to the test box, and behavior was video-recorded for 60 min. Videos were scored using a time-sampling procedure in which the presence of licking or biting of the injected paw was recorded during the first 10 s of every min for a total of 60 observations per mouse. We based this procedure on that used by Chesler et al.[74], where formalin behavior was quantified using a similar time-sampling procedure that can be seen in Fig. 2 of that paper. Formalin hind paw injection typically presents a pattern of vigorous licking in the first 5–10 min, deemed the "early phase," a quiescent period in the next 5–10 min where very little licking occurs, then a "late phase" of sporadic licking that occurs throughout the remainder of the testing period[75,76]. While total time spent licking is often reported in formalin studies, the time-sampling approach used here has been used by our labs across several studies and provides reliable quantification of nocifensive behavior[77–81]. Accordingly, formalin data are presented as the percentage of positive samples across the late phase of the test.

Hot plate thermal sensitivity test

The hot plate test was used to assess whether applying CCK to the dmPAG or lPAG enhanced thermal sensitivity. Mice were tested in a counterbalanced manner on the hot plate 30 min after microinfusion with CCK or aCSF, then 48 h later were retested with the other drug. After microinfusion, mice were immediately moved to the testing room. Mice were then placed singly on a clean hot plate set at 52.5 °C for 45 s. Videos were analyzed using BORIS (Behavioral Observation Research Interactive Software, v7.13.9)[82] for the latency to first hind paw flick, lick, or jump.

Quantification of social behavior

In a subset of mice, behaviors during the 30-min one-in-pain social interaction were scored. Behaviors were sampled during the first 10 s of every minute. Data were quantified as the percent positive samples across the 30 min session. In the demonstrator mouse, we recorded hind paw licking. In the observer mouse, we recorded: (1) attending

toward the cagemate, including sniffing or grooming, excluding the anogenital region, and (2) propinquity behavior defined as being within 2 cm or less of the demonstrator mouse, but not actively engaging in attending behavior.

Open field

Mice were placed in the center of a white open field box (42 cm × 42 cm × 42 cm) and recorded for 10 min (EthoVision XT v.11.5, Noldus Information Technology, Leesburg VA). Total distance traveled and velocity data were collected as measures of the effect of intra-lPAG proglumide infusion on motor responses. Mice were tested without infusion (day 1), 48 h later with proglumide infusion (day 2), and again 48 h later without infusion (day 3).

Surgical procedures

All surgeries were performed under sterile conditions and isoflurane anesthesia (4% induction, 2–2.5% maintenance). Body temperature was maintained using a circulating heated water mat.

Hind paw incision surgery

A 5-mm incision through the skin and fascia was performed on the left hind paw of the mouse[83]. The flexor digitorum brevis muscle was elevated with forceps or a blunt dissection probe, and a longitudinal incision was made through the muscle by a scalpel. The wound was closed with two skin sutures.

Chronic constriction injury (CCI) surgery

The sciatic nerve was exposed midway along the thigh using gentle dissection through the biceps femoris muscle. Proximal to the trifurcation of the sciatic nerve, approximately 7 mm of nerve tissue was released from surrounding tissue. Three ligatures (7-0 silicone-coated braided silk, Sofsilk) were loosely tied around the nerve, spaced roughly 1 mm apart. The affected nerve segment measured between 4 and 5 mm in length. Particular attention was paid to tying the ligatures to ensure minimal constriction of the nerve when examined under ×40 magnification. The intended level of constriction impeded, but did not fully halt, circulation through the outer blood vessels of the nerve, occasionally eliciting a brief muscle twitch around the exposed area. The incision was subsequently closed in layers. This assay mimics neuropathic pain states in humans and causes hypersensitivity lasting more than a month[84,85].

Stereotaxic surgery

The scalp was sterilized, shaved, a small incision was made in the skin, the skull leveled using a digital stereotaxic instrument (Harvard Apparatus, Holliston, MA), and burr holes drilled at the respective stereotaxic coordinates. Viral vectors or cannulae were lowered to the target sites, the incision was closed, and mice received postsurgical analgesia (meloxicam, 20 mg/kg) once daily for 3 days.

Cannulations and microinfusion experiments

Mice were cannulated with either a single cannula for drug application to the dmPAG or a double cannula for bilateral drug application to the lPAG. Separate cohorts of mice for both region and drug were used and then tested on either the von Frey or hot plate tests. A single guide cannula with length 3.0 mm and injector cut 0.5 mm below the pedestal (C315GS-5/spc, P1 Technologies, Roanoke, VA) was implanted above the dmPAG (11.7° angle, AP −3.6 mm, ML −0.2 mm, DV −2.55 mm), or a double guide cannula (RWD Life Science, San Diego, CA: guide cannula 62056, center distance 1.4 mm, length 3.0 mm, dummy 62127, injector 62056, both cut 0.5 mm below guide cannula, cap 62525) was implanted above the lPAG (AP −3.85 mm, ML ±0.55 mm, DV −2.65 mm) at 7 weeks of age. Following a 7-day recovery period, mice were tested for baseline von Frey sensitivity and then either underwent contextual nocebo or social nocebo procedures (see above). In all experiments, microinfusions were performed under light isoflurane anesthesia immediately preceding context exposure or the 1-h habituation before social nocebo. In Fig. 3d–i, infusions occurred 30–45 min before pain testing. During infusion, calibrated tubing was used to connect the internal cannula to a microliter syringe (1700 series Hamilton Syringe, 100 µl, Harvard Apparatus, Montreal QC), and an infusion pump (Pump 11 Elite Nanomite, Harvard Apparatus, Montreal QC) was used to infuse a 0.25-µl volume over 5 min (50 nl/min), after which the injector was left in place for an additional 1 min. Mice were allowed to recover in their home cage prior to testing. Cannula placement was verified post hoc by infusing 250 nl of fluorescent muscimol-BODIPY (M23400, Invitrogen) and quantifying the radial spread of fluorescence for both dmPAG (single cannula) and lPAG (bilateral cannula) experiments. The estimated spread radius was approximately 300–350 µm and was comparable across hemispheres in bilateral infusions and similar in magnitude to single-cannula infusions. Mice with placements outside the intended target region (dmPAG or lPAG) were excluded (<5%).

Viral infusions

Viruses were infused at a rate of 60 nl/min using a glass capillary micropipette backfilled with mineral oil and attached to a 1700 series gas-tight Hamilton microsyringe. Micropipettes were lowered 0.1 mm below the injection site (ACC: AP +1.0 mm, ML ±0.5 mm, DV −0.8 mm; lPAG: AP −3.85 mm, ML ±0.5 mm, DV −2.65 mm) prior to infusion and left in position for 10 min prior to slow removal to prevent backflow. Skin was sutured, and the mouse recovered on a heated pad. Viruses were allowed 3 weeks of expression prior to behavioral testing or tracing.

Optogenetic manipulations

CCK-IRES-Cre mice were infused with a virus expressing eOPN3, ChR2, or control in the lPAG. In the same surgery session, an optic fiber cannula (200 µm core, 3.0 mm length, R-FOC-BL200C-39NA, RWD Life Science, San Diego, CA) was implanted above the lPAG and secured with dental cement (3M ESPE RelyX Unicem Aplicap Self-Adhesive Universal Resin Cement, 56818). The virus was allowed to express for 3 weeks. For the contextual nocebo eOPN3 experiments, viruses were injected 2 weeks prior to baseline, followed by hind paw incision surgery and conditioning to the cubicles. This allowed the virus to express for a total of 3 weeks before mice were tested on test day. In addition, mice were connected to the patch cord (200 nm, Doric, Quebec City, QC) for 10 min at the beginning of the 5-h conditioning period in the contextual nocebo experiments. Then, on the test day, mice were tethered and immediately put into the observation box, exposed to that box for 30 min, then put into the von Frey cubicle and allowed to rest for 10 min. They were then tested for mechanical sensitivity using the manual von Frey test. For the social nocebo paradigm, mouse pairs were habituated to the box for 1 h. One day prior to testing, pairs were habituated again to the box for 30 min, then the observer mouse was habituated to the patch cord in the box for 10 min. On test day, pairs were habituated for 1 h to the container, then the patch cord was attached to the observer mouse that was allowed to further acclimate for 5 min.

Optical stimulation for eOPN3

Light delivery was initiated immediately after placement in the conditioning box for contextual nocebo or following formalin injection in the demonstrator for social nocebo. Optical stimulation consisted of 50 ms pulses at a light power density of 10 mW/mm^2 of 470 nm light (470 nm, 50 W Collimated LED BLS-LCS-0470-50-22, Oasis Implant, Polyscan3 software, Mightex, Toronto, Canada) delivered once every 2 min to the lPAG of the conditioned mouse or observer for the 30 min duration. Mice were then moved to individual Plexiglas cubicles over a metal mesh platform and tested for mechanical sensitivity. Values

reported are the average of two measures on each hind paw. In one experiment, light was delivered in 10-min epochs spaced at 1 h intervals throughout conditioning to minimize tissue heating and phototoxicity during prolonged inhibition.

Optical stimulation for ChR2

Mice were tested for baseline mechanical sensitivity. Mice were then habituated to the stimulation box for 30 min during two consecutive days prior to testing, with 10 min of habituation to the patch cord each day. On test day, mice were habituated to the box with a patch cord for 10 min prior to stimulation. For optogenetic photostimulation of ChR2, light output was 10 mW/mm^2 delivered at cycles of 5 ms bursts of light on and 45 ms of light off for a frequency stimulation of 20 Hz over a 3 min period. Mice were immediately removed from the stimulation box and placed in von Frey cubicles. In one experiment, mice were tested using manual von Frey, and values reported represent the average of two measures on the left hind paw. In another experiment, mice were tested using electronic von Frey with the baseline representing the average of three measures, and then subsequent time points (5, 15, 30, 45, 60, 90, and 120 min post-stimulation) are a single measure per hind paw.

Pharmacological agents

Proglumide (10 mg/kg; Sigma Aldrich, Oakville, ON) was dissolved in saline and administered intraperitoneally (i.p.). LY 225910, the CCK-2 antagonist (1 mg/kg, Tocris, Burlington, ON), was dissolved in 5% DMSO in saline using a sonicator or 5% DMSO and 0.5% Tween-80 in saline and administered intraperitoneally (i.p.). Systemically administered drugs were injected using a volume of 10 ml/kg body weight. In microinfusion experiments, proglumide (250 ng in 250 nl aCSF, Sigma Aldrich) or CCK-sulfated octapeptide (CCK-8S) (50 ng in 250 nl aCSF, Cayman Chemicals, Ann Arbor, MI) were microinfused through implanted cannulas via calibrated tubing (see below).

Viral reagents

Viruses were injected at a volume of 200 nl for functional experiments and 100 nl for tracing. AAVretro-CAG-DIO-mNeptune, AAV2/9-hSyn-SIO-eOPN3-mScarlet, AAV2/9-Ef1a-DIO-ChR2(H134R)-mCherry, and AAV2/9-EF1a-DIO-mCherry were purchased from Neurophotonics (Quebec City, QC). AAV2/8-hSyn-DIO-mCherry, AAV2/8-hSyn-DIO-hM4D(Gi)-mCherry, AAV2/8-CaMKIIa-hM4D(Gi)-mCherry, and AAV-2/8-CaMKIIa-GFP were purchased from Addgene (Watertown, MA).

Tissue preparation and immunohistochemistry

Mice were deeply anesthetized with sodium pentobarbital (100 mg/kg, i.p.) and underwent transcardiac perfusion with 0.1 M phosphate-buffered saline (PBS, pH = 7.4) followed by 4% (w/v) paraformaldehyde in PBS (PFA). Brain tissue was extracted and post-fixed for 24 h in 4% PFA, then cryoprotected for 48 h in 30% (w/v) sucrose. Tissue was embedded in cutting medium (Tissue-Plus O.C.T. Compound, Fisher Scientific Canada) and frozen. Frozen tissue was then sectioned coronally on a cryostat (Cryostar NX50, ThermoFisher Scientific) at 40 µm thickness, then collected in cryoprotectant (30% w/v sucrose, 30% v/v ethylene glycol, 0.1 M PBS) until use. Sections were thawed, placed in a 12-well plate, then washed three times for 5 min in 0.1 M PBS (pH 7.4). Sections were blocked (5% normal goat serum, 0.3% Triton X-100, 0.1 M PBS) for 2 h at room temperature (RT). The block was removed, and sections were then incubated in the primary antibody at 4 °C. For c-Fos studies, a rabbit monoclonal antibody (rabbit α c-Fos 1:10,000 for 48 h, Synaptic Systems 226008, Göttingen, Germany) was used. In the retrograde tracing experiment, a monoclonal NeuN antibody (1:2,000 overnight, EMD Millipore MABN140, Darmstadt, Germany) or a polyclonal EMX1 antibody (1:50 overnight, Invitrogen, PA5-35373, Carlsbad, CA), were used as general or excitatory neuronal markers, respectively. Following primary antibody incubation, sections were washed three times for 5 min in PBS, then incubated with secondary antibody (c-Fos experiments: goat anti-rabbit, 1:500, 2 h at RT, Vector Laboratories DI-1649-1.5, Newark, CA; NeuN and EMX1 experiments: goat anti-rabbit Alexa Fluor 488, 1:500, 2 h at RT, Invitrogen A11008, Waltham, MA). Sections were then washed three times for 5 min in PBS, mounted on Superfrost slides, and dipped in DAPI solution (1:50,000 in 0.1 M PBS, 5 min, D9542, Sigma Aldrich Canada, Oakville, ON) and coverslipped with mounting medium (Fluoromount-G, SouthernBiotech, Birmingham, AL).

Imaging and analysis of c-Fos

Digital images of coronal brain sections were taken at 4× (1.6125 µm/pixel, Biotek Cytation 5, Gen5 software v3.03, Agilent, Santa Clara, CA) for the social nocebo paradigm or 10× (Olympus VS200 slide scanner, VS-ASW software v3.4.1, Evident Corporation, Tokyo, Japan) for the contextual nocebo paradigm. QuPath (v0.3.2)[86] was used along with the Allen Mouse Brain Reference Atlas Version 2 (Allen Institute for Brain Science, 2011) and a schematic of the columns of the rat PAG[87] to draw regions of interest (ROI) around the anterior, intermediate, and posterior PAG. In addition, we used the DAPI channel to visualize changes in cell density that distinguish the columnar organization of the PAG. c-Fos-positive cells were identified based on high grayscale signal and oval-shaped nuclei using the QuPath cell detection feature, followed by manual addition and subtraction of cells by researchers blinded to the condition. c-Fos-positive regions were quantified and reported as the number of cells/mm^2, and at least three sections between the bregma range were averaged for each ROI. An unbiased approach was taken, such that sections from the anterior, intermediate, and posterior PAG as follows: anterior PAG: between bregma −2.3 and −2.6. Intermediate PAG: between bregma −3.6 and −3.9. Posterior PAG: between bregma −4.7 and −4.9. For cortical analyses, c-Fos quantification was performed separately across cortical layers (L1, L2/3, L5, and L6) and for retrogradely labeled neurons to distinguish general cortical activation from activation within projection-defined populations.

Retrograde tracer and NeuN/EMX1 analysis

The density of CCK-positive (tagged by virus) to NeuN/EMX1-positive cells was compared between selected brain regions (average of 3 slices per mouse from 3 mice for EMX1, average of 3 slices per mouse from 3 mice for NeuN). Digital images of coronal brain sections were taken at 10× (Olympus VS200 slide scanner) using filters for DAPI, GFP (NeuN/EMX1), and mCherry (retrograde virus). QuPath was used along with the Allen Mouse Brain Reference Atlas Version 2 (Allen Institute for Brain Science, 2011) to draw regions of interest (ROI) in the ACC (AP +0.9 to +1.15, ACAd and ACAv), insula (AP +0.9 to +1.15, AId and AIv), motor cortex (AP −1.25 to −0.95, MOs and MOp), retrosplenial cortex (RSPd and RSPv combined), parietal cortex (AP −2.35 to −2.15, PTLp), and lPAG (AP −3.9 to −3.7). Quantification boundaries were drawn around layer V in each cortical region because retrogradely labeled cells were most abundant in this layer. NeuN-positive cells were identified based on high grayscale signal and oval-shaped nuclei using the QuPath cell detection feature, followed by manual addition and subtraction of cells, whereas mCherry-positive (CCK$^+$) cells were quantified using the manual point counting feature. CCK cell density was calculated as a percentage of the mCherry-positive cells within the ROI (mm^2) relative to the total number of NeuN-positive cells within the ROI. Density counts were averaged across three consecutive coronal slices for each ROI.

RNAscope

Tissue was collected and cut at 40 µm free-floating and then mounted on Superfrost Plus Gold slides. The RNAscope Multiplex Fluorescent V2 Assay (Advanced Cell Diagnostics (ACD), Inc., Newark, CA) was performed according to manufacturer instructions (UM 323100) using

the fixed-frozen tissue sample pretreatment and RNAscope Protease III. Tissue was probed for *Cckbr* (CCK-2 receptor, ACD probe cat no. 439121) and *Fos* (ACD probe cat no. 316921) mRNA and respective 570 and 690 nm opal dyes (Akoya Biosciences). Slides were coverslipped with ProLong Gold mounting media (Invitrogen, Waltham, MA) and imaged within one week at 20X (Olympus VS200 slide scanner, Evident Corporation, Tokyo, Japan). We report active cells that express *Cckbr* in the social nocebo and contextual nocebo paradigms as the percent of *Fos*-positive cells (distinct 690 nm-positive ovals) that also express *Cckbr* (at least three 570 nm dots within a *Fos*-positive cell boundary). Transcriptomic reference data (see Supplementary Fig. 16) indicated that *Cckbr* expression in the PAG is predominantly neuronal, with most expressing glutamatergic markers, and therefore, additional neuronal marker co-staining was not performed.

Verification of viral injections

For verification of viral injections, sections were processed as described above. Injection location was considered accurate when the expression of the virus was limited to the boundaries of the target brain region. When visualization of the virus was not possible or the spread of the virus was beyond the designated target, data were not included. This occurred in less than 5% of the injected mice.

Analysis of publicly available transcriptomic datasets

To provide molecular context for *Cckbr*-expressing neurons in the PAG, we analyzed publicly available whole-brain single-cell and spatial transcriptomic datasets from the Allen Brain Cell Atlas[44]. Neuronal subclasses within the PAG were identified using the reference taxonomy provided by the Allen Institute, and expression of *Cckbr* was quantified across neuronal populations and along the rostral-caudal axis. Co-expression analyses were performed for genes associated with neuromodulatory and pain-related signaling pathways. These analyses were used to determine the distribution of *Cckbr* across molecularly defined PAG neuronal populations rather than to define cell identity within individual experimental animals.

Statistical analyses

Statistical analyses were performed using SPSS (v28, IBM) with an α level of 0.05. Depending on the design, data were analyzed using one-way ANOVA, repeated-measures ANOVA, or two-tailed t-tests. Full statistical details for the main figures are provided in Supplementary Data 1 and in the corresponding figure legends for Supplementary Figs. When ANOVAs were significant, Šidák or Tukey multiple-comparison tests were applied as appropriate. For box plots, the box represents the interquartile range (Q1–Q3), the center line denotes the median, and whiskers indicate the minimum and maximum values. Graphical figures were generated using GraphPad Prism (v9), Adobe Illustrator (v27.7), and templates adapted from BioRender.com.

Reproducibility

All experiments were conducted in at least two independent cohorts. Behavioral testing was performed across multiple cohorts ($n = 6$–10 mice per cohort; $n = 3$–4 per group), each serving as an independent replication, with consistent findings across cohorts and laboratories. Experimenters were blind to the experimental condition and manipulation. Quantification of c-Fos/ICC labeling was performed independently by at least two blinded experimenters.

Reporting summary

Further information on research design is available in the Nature Portfolio Reporting Summary linked to this article.

Data availability

The data generated in this study are provided in the Supplementary Information/Source data file. Source data are provided with this paper.

References

1. Testa, M., Rossettini, G., Barbiani, D. & Miciak, M. *Placebo Effects Through the Lens of Translational Research* (eds Colloca, L. et al.) Vol. 0 (Oxford University Press, 2023).
2. Vogtle, E., Barke, A. & Kroner-Herwig, B. Nocebo hyperalgesia induced by social observational learning. *Pain* **154**, 1427–1433 (2013).
3. Colloca, L. & Benedetti, F. Placebo analgesia induced by social observational learning. *Pain* **144**, 28–34 (2009).
4. Tracey, I. Getting the pain you expect: mechanisms of placebo, nocebo and reappraisal effects in humans. *Nat. Med.* **16**, 1277–1283 (2010).
5. Benedetti, F., Mayberg, H. S., Wager, T. D., Stohler, C. S. & Zubieta, J. K. Neurobiological mechanisms of the placebo effect. *J. Neurosci.* **25**, 10390–10402 (2005).
6. Zunhammer, M., Spisak, T., Wager, T. D., Bingel, U. & Placebo Imaging, C. Meta-analysis of neural systems underlying placebo analgesia from individual participant fMRI data. *Nat. Commun.* **12**, 1391 (2021).
7. Chen, C. et al. Neural circuit basis of placebo pain relief. *Nature* **632**, 1092–1100 (2024).
8. Neyama, H. et al. Opioidergic activation of the descending pain inhibitory system underlies placebo analgesia. *Sci. Adv.* **11**, eadp8494 (2025).
9. Colloca, L. The nocebo effect. *Annu. Rev. Pharmacol. Toxicol.* **64**, 171–190 (2024).
10. Benedetti, F., Amanzio, M., Casadio, C., Oliaro, A. & Maggi, G. Blockade of nocebo hyperalgesia by the cholecystokinin antagonist proglumide. *Pain* **71**, 135–140 (1997).
11. Benedetti, F., Amanzio, M. & Maggi, G. Potentiation of placebo analgesia by proglumide. *Lancet* **346**, 1231 (1995).
12. Martin, L. J. et al. Male-specific conditioned pain hypersensitivity in mice and humans. *Curr. Biol.* **29**, 192–201 (2019).
13. Jee, H. J. et al. Anterior cingulate cortex regulates pain catastrophizing-like behaviors in rats. *Mol. Brain* **16**, 71 (2023).
14. Smith, M. L., Asada, N. & Malenka, R. C. Anterior cingulate inputs to nucleus accumbens control the social transfer of pain and analgesia. *Science* **371**, 153–159 (2021).
15. Laviola, G. et al. Low empathy-like behaviour in male mice associates with impaired sociability, emotional memory, physiological stress reactivity and variations in neurobiological regulations. *PLoS ONE* **12**, e0188907 (2017).
16. Colloca, L., Petrovic, P., Wager, T. D., Ingvar, M. & Benedetti, F. How the number of learning trials affects placebo and nocebo responses. *Pain* **151**, 430–439 (2010).
17. Qu, C. et al. Lesion of the rostral anterior cingulate cortex eliminates the aversiveness of spontaneous neuropathic pain following partial or complete axotomy. *Pain* **152**, 1641–1648 (2011).
18. Foltz, E. L. & White, L. E. Jr. Pain "relief" by frontal cingulumotomy. *J. Neurosurg.* **19**, 89–100 (1962).
19. Li, M. et al. The mPFC-PAG in defensive coping: a correlational but not causal role in shifting strategy. *Behav. Brain Res.* **502**, 116037 (2026).
20. Bliss-Moreau, E., Santistevan, A. C., Bennett, J., Moadab, G. & Amaral, D. G. Anterior cingulate cortex ablation disrupts affective vigor and vigilance. *J. Neurosci.* **41**, 8075–8087 (2021).
21. Fiddick, L. There is more than the amygdala: potential threat assessment in the cingulate cortex. *Neurosci. Biobehav. Rev.* **35**, 1007–1018 (2011).
22. Legrain, V., Iannetti, G. D., Plaghki, L. & Mouraux, A. The pain matrix reloaded: a salience detection system for the body. *Prog. Neurobiol.* **93**, 111–124 (2011).
23. Shih, Y. W. et al. Effects of positive and negative expectations on human pain perception engage separate but interrelated and dependently regulated cerebral mechanisms. *J. Neurosci.* **39**, 1261–1274 (2019).

24. Calejesan, A. A., Kim, S. J. & Zhuo, M. Descending facilitatory modulation of a behavioral nociceptive response by stimulation in the adult rat anterior cingulate cortex. *Eur. J. Pain.* **4**, 83–96 (2000).
25. Zhuo, M. Descending facilitation. *Mol. Pain.* **13**, 1744806917699212 (2017).
26. Crawford, L. S. et al. Brainstem mechanisms of pain modulation: a within-subjects 7T fMRI study of placebo analgesic and nocebo hyperalgesic responses. *J. Neurosci.* **41**, 9794–9806 (2021).
27. Trask, S., Mogil, J. S., Helmstetter, F. J., Stucky, C. L. & Sadler, K. E. Contextual control of conditioned pain tolerance and endogenous analgesic systems: evidence for sex-based differences in endogenous opioid engagement. *eLife* **11**, e75283 (2022).
28. Brascher, A. K., Kleinbohl, D., Holzl, R. & Becker, S. Differential classical conditioning of the nocebo effect: increasing heat-pain perception without verbal suggestions. *Front. Psychol.* **8**, 2163 (2017).
29. Saunders, C., Colagiuri, B. & Barnes, K. Socially acquired nocebo effects generalize but are not attenuated by choice. *Ann. Behav. Med.* **57**, 1069–1080 (2023).
30. Martin, L. J. et al. Reducing social stress elicits emotional contagion of pain in mouse and human strangers. *Curr. Biol.* **25**, 326–332 (2015).
31. Langford, D. J. et al. Social modulation of pain as evidence for empathy in mice. *Science* **312**, 1967–1970 (2006).
32. Lidhar, N. K. et al. Prelimbic cortex glucocorticoid receptors regulate the stress-mediated inhibition of pain contagion in male mice. *Neuropsychopharmacology* **46**, 1183–1193 (2021).
33. Li, Z. et al. Social interaction with a cagemate in pain facilitates subsequent spinal nociception via activation of the medial prefrontal cortex in rats. *Pain* **155**, 1253–1261 (2014).
34. Colloca, L. & Benedetti, F. Nocebo hyperalgesia: how anxiety is turned into pain. *Curr. Opin. Anaesthesiol.* **20**, 435–439 (2007).
35. Baumbach, J. L., Mui, C. Y. Y., Leonetti, A. M. & Martin, L. J. A history of injury enhances affective and sensory responses to predator threat by sensitizing corticosterone release through TRPA1 receptor signaling. *Curr. Biol.* **35**, 3896–3907 (2025).
36. Baumbach, J. L., Mui, C. Y. Y., Leonetti, A. M. & Martin, L. J. Corticosterone regulates the balance between freezing and rearing in defensive responses to predator threat. *Prog. Neuropsychopharmacol. Biol. Psychiatry* **144**, 111579 (2025).
37. Borelli, K. G. & Brandao, M. L. Effects of ovine CRF injections into the dorsomedial, dorsolateral and lateral columns of the periaqueductal gray: a functional role for the dorsomedial column. *Horm. Behav.* **53**, 40–50 (2008).
38. Bandler, R. & Depaulis, A. *The Midbrain Periaqueductal Gray Matter: Functional, Anatomical, and Neurochemical Organization* (eds Depaulis, A. & Bandler, R.) 175–198 (Springer, 1991).
39. Liu, Y. et al. A circuit from dorsal hippocampal CA3 to parvafox nucleus mediates chronic social defeat stress-induced deficits in preference for social novelty. *Sci. Adv.* **8**, eabe8828 (2022).
40. Kaneko, T. et al. Orexin neurons play contrasting roles in itch and pain neural processing via projecting to the periaqueductal gray. *Commun. Biol.* **7**, 290 (2024).
41. Johnson, S. B. et al. Activity in a prefrontal-periaqueductal gray circuit overcomes behavioral and endocrine features of the passive coping stress response. *Proc. Natl. Acad. Sci. USA* **119**, e2210783119 (2022).
42. Moran, T. H., Robinson, P. H., Goldrich, M. S. & McHugh, P. R. Two brain cholecystokinin receptors: implications for behavioral actions. *Brain Res.* **362**, 175–179 (1986).
43. Lein, E. S. et al. Genome-wide atlas of gene expression in the adult mouse brain. *Nature* **445**, 168–176 (2007).
44. Yao, Z. et al. A high-resolution transcriptomic and spatial atlas of cell types in the whole mouse brain. *Nature* **624**, 317–332 (2023).
45. Baumbach, J. L., Mui, C. Y. Y., Tuz Zahra, F. & Martin, L. J. A single exposure to the predator odor 2,4,5-trimethylthiazoline causes long-lasting affective behavioral changes in female mice: modulation by kappa opioid receptor signaling. *Pharmacol. Biochem. Behav.* **242**, 173822 (2024).
46. Benedetti, F., Amanzio, M., Vighetti, S. & Asteggiano, G. The biochemical and neuroendocrine bases of the hyperalgesic nocebo effect. *J. Neurosci.* **26**, 12014–12022 (2006).
47. Becker, C. et al. Repeated social defeat-induced depression-like behavioral and biological alterations in rats: involvement of cholecystokinin. *Mol. Psychiatry* **13**, 1079–1092 (2008).
48. Andre, J. et al. Involvement of cholecystokininergic systems in anxiety-induced hyperalgesia in male rats: behavioral and biochemical studies. *J. Neurosci.* **25**, 7896–7904 (2005).
49. Zhang, Y. et al. A new experimental rat model of nocebo-related nausea involving double mechanisms of observational learning and conditioning. *CNS Neurosci. Ther.* **30**, e14389 (2024).
50. Zou, M., Li, S., Klein, W. H. & Xiang, M. Brn3a/Pou4f1 regulates dorsal root ganglion sensory neuron specification and axonal projection into the spinal cord. *Dev. Biol.* **364**, 114–127 (2012).
51. Ray, P. et al. Comparative transcriptome profiling of the human and mouse dorsal root ganglia: an RNA-seq-based resource for pain and sensory neuroscience research. *Pain* **159**, 1325–1345 (2018).
52. Lee, J. Y. et al. Role of anterior cingulate cortex inputs to periaqueductal gray for pain avoidance. *Curr. Biol.* **32**, 2834–2847 (2022).
53. Asim, M., Wang, H., Waris, A., Qianqian, G. & Chen, X. Cholecystokinin neurotransmission in the central nervous system: insights into its role in health and disease. *Biofactors* **50**, 1060–1075 (2024).
54. Deng, P. Y. et al. Cholecystokinin facilitates glutamate release by increasing the number of readily releasable vesicles and releasing probability. *J. Neurosci.* **30**, 5136–5148 (2010).
55. Bernard, A. et al. The cholecystokinin type 2 receptor, a pharmacological target for pain management. *Pharmaceuticals* **14**, https://doi.org/10.3390/ph14111185 (2021).
56. Hebb, A. L., Poulin, J. F., Roach, S. P., Zacharko, R. M. & Drolet, G. Cholecystokinin and endogenous opioid peptides: interactive influence on pain, cognition, and emotion. *Prog. Neuropsychopharmacol. Biol. Psychiatry* **29**, 1225–1238 (2005).
57. Levine, J. D., Gordon, N. C. & Fields, H. L. The mechanism of placebo analgesia. *Lancet* **2**, 654–657 (1978).
58. Benedetti, F., Amanzio, M. & Thoen, W. Disruption of opioid-induced placebo responses by activation of cholecystokinin type-2 receptors. *Psychopharmacology* **213**, 791–797 (2011).
59. Livrizzi, G. et al. Top-down control of the descending pain modulatory system drives placebo analgesia. *Neuron* S0896-6273(26)00216-3. https://doi.org/10.1016/j.neuron.2026.03.025 (2026). Online ahead of print.
60. Kimmey, B. A. et al. Convergent state-control of endogenous opioid analgesia. Preprint at *bioRxiv* https://doi.org/10.1101/2025.01.03.631111 (2025).
61. Seymour, B. Pain: a precision signal for reinforcement learning and control. *Neuron* **101**, 1029–1041 (2019).
62. Krahe, C., Springer, A., Weinman, J. A. & Fotopoulou, A. The social modulation of pain: others as predictive signals of salience—a systematic review. *Front. Hum. Neurosci.* **7**, 386 (2013).
63. Cho, C., Deol, H. K. & Martin, L. J. Bridging the translational divide in pain research: biological, psychological and social considerations. *Front. Pharmacol.* **12**, 603186 (2021).
64. Martin, L. J., Tuttle, A. H. & Mogil, J. S. The interaction between pain and social behavior in humans and rodents. *Curr. Top. Behav. Neurosci.* **20**, 233–250 (2014).
65. Mogil, J. S. The translatability of pain across species. *Philos. Trans. R. Soc. B Biol. Sci.* **374**, 20190286 (2019).

66. Colloca, L. & Finniss, D. Nocebo effects, patient-clinician communication, and therapeutic outcomes. *JAMA* **307**, 567–568 (2012).
67. Corsi, N. & Colloca, L. Placebo and nocebo effects: the advantage of measuring expectations and psychological factors. *Front. Psychol.* **8**, 308 (2017).
68. Manai, M., van Middendorp, H., Veldhuijzen, D. S., Huizinga, T. W. J. & Evers, A. W. M. How to prevent, minimize, or extinguish nocebo effects in pain: a narrative review on mechanisms, predictors, and interventions. *Pain Rep.* **4**, e699 (2019).
69. Sorge, R. E. et al. Olfactory exposure to males, including men, causes stress and related analgesia in rodents. *Nat. Methods* **11**, 629–632 (2014).
70. Li, C. L. et al. Validating rat model of empathy for pain: effects of pain expressions in social partners. *Front. Behav. Neurosci.* **12**, 242 (2018).
71. Chaplan, S. R., Bach, F. W., Pogrel, J. W., Chung, J. M. & Yaksh, T. L. Quantitative assessment of tactile allodynia in the rat paw. *J. Neurosci. Methods* **53**, 55–63 (1994).
72. Hargreaves, K., Dubner, R., Brown, F., Flores, C. & Joris, J. A new and sensitive method for measuring thermal nociception in cutaneous hyperalgesia. *Pain* **32**, 77–88 (1988).
73. Rosland, J. H., Tjolsen, A., Maehle, B. & Hole, K. The formalin test in mice: effect of formalin concentration. *Pain* **42**, 235–242 (1990).
74. Chesler, E. J. et al. Genotype-dependence of gabapentin and pregabalin sensitivity: the pharmacogenetic mediation of analgesia is specific to the type of pain being inhibited. *Pain* **106**, 325–335 (2003).
75. Coderre, T. J., Fundytus, M. E., McKenna, J. E., Dalal, S. & Melzack, R. The formalin test: a validation of the weighted-scores method of behavioural pain rating. *Pain* **54**, 43–50 (1993).
76. Fischer, M., Carli, G., Raboisson, P. & Reeh, P. The interphase of the formalin test. *Pain* **155**, 511–521 (2014).
77. Martin, L. J. et al. Differences in the antinociceptive effects and binding properties of propranolol and bupranolol enantiomers. *J. Pain*, https://doi.org/10.1016/j.jpain.2015.09.004 (2015).
78. Martin, L. J. et al. Epiregulin and EGFR interactions are involved in pain processing. *J. Clin. Investig.* **127**, 3353–3366 (2017).
79. Khoutorsky, A. et al. Translational control of nociception via 4E-binding protein 1. *eLife* **4**, https://doi.org/10.7554/eLife.12002 (2015).
80. Wieskopf, J. S. et al. Broad-spectrum analgesic efficacy of IBNtxA is mediated by exon 11-associated splice variants of the mu-opioid receptor gene. *Pain* **155**, 2063–2070 (2014).
81. Martin, L. J. et al. Altered nociceptive behavior and emotional contagion of pain in mouse models of autism. *Genes Brain Behav.* **21**, e12778 (2022).
82. Friard, O. & Gamba, M. BORIS: a free, versatile open-source event-logging software for video/audio coding and live observations. *Methods Ecol. Evol.* **7**, 1325–1330 (2016).
83. Cowie, A. M. & Stucky, C. L. A mouse model of postoperative pain. *Bio Protoc.* **9**, https://doi.org/10.21769/BioProtoc.3140 (2019).
84. Zumbusch, A. S., McEachern, E. L. F., Morgan, O. B., Nickner, E. & Mogil, J. S. Normative preclinical algesiometry data on the von Frey and radiant heat paw-withdrawal tests: an analysis of data from more than 8,000 mice over 20 years. *J. Pain* **25**, 104468 (2024).
85. Bennett, G. J. & Xie, Y. K. A peripheral mononeuropathy in rat that produces disorders of pain sensation like those seen in man. *Pain* **33**, 87–107 (1988).
86. Bankhead, P. et al. QuPath: open source software for digital pathology image analysis. *Sci. Rep.* **7**, 16878 (2017).
87. Keay, K. & Bandler, R. *The Senses: A Comprehensive Reference* (eds Masland, R. H. et al.) 627–634 (Academic Press, 2008).

Acknowledgements

This work was supported by the Canadian Institutes of Health Research PJT—189987 (L.J.M.) and Foundation Grant 154281 (J.S.M.), the Natural Sciences and Engineering Research Council of Canada RGPIN-2023-05350 (L.J.M.), and the Canada Research Chairs Program (L.J.M.). S.J.P. was supported by a University of Toronto Center for the Study of Pain Fellowship. A.S. was supported by a Rubicon grant from the Dutch Research Council.

Author contributions

S.J.P., J.S.M., and L.J.M. conceptualized and designed the study. S.J.P., A.S., F.T.Z., D.C.B., S.A.K., L.V.P., W.C., A.M., J.B., Z.S., M.I.F., S.G., O.B.M., M.D., A.D., L.L., R.C., and L.J.M. performed the experiments and collected the data. S.J.P., L.J.M. prepared the figures. J.S.M., L.J.M. supervised the project and acquired funding. L.J.M. wrote the original draft, with contributions from S.J.P., A.S., and J.S.M.

Competing interests

The authors declare no competing interests.

Additional information

Supplementary information The online version contains Supplementary material available at https://doi.org/10.1038/s41467-026-73266-y.

Correspondence and requests for materials should be addressed to Jeffrey S. Mogil or Loren J. Martin.

Peer review information *Nature Communications* thanks Ewelina Knapska, Monique Smith, and the other anonymous reviewer(s) for their contribution to the peer review of this work. A peer review file is available.